DNA methylation-environment interactions in the human genome

Rachel A. Johnston[1,2,3], Katherine A. Aracena[4], Luis B. Barreiro[4,5,6], Amanda J. Lea[7,8], Jenny Tung[1,8, 9,10,11]

[1]Department of Evolutionary Anthropology, Duke University, Durham, NC 27708, USA
[2]Zoo New England, Boston, MA 02121, USA
[3]Broad Institute of MIT and Harvard, Cambridge, MA 02142, USA
[4]Department of Human Genetics, University of Chicago, Chicago, IL 60637, USA
[5]Section of Genetic Medicine, Department of Medicine, University of Chicago, Chicago, IL 60637, USA
[6]Committee on Immunology, University of Chicago, Chicago, IL 60637, USA
[7]Department of Biological Sciences, Vanderbilt University, Nashville, TN 37240, USA
[8]Canadian Institute for Advanced Research, Toronto, Canada M5G 1Z8
[9]Duke Population Research Institute, Duke University, Durham, NC 27708, USA
[10]Department of Biology, Duke University, Durham, NC 27708, USA
[11]Department of Primate Behavior and Evolution, Max Planck Institute for Evolutionary Anthropology, 04103 Leipzig, Saxony, Germany

*Corresponding author: E-mail: jtung@eva.mpg.de; racheljohnston7@gmail.com

Abstract

Previously we showed that a massively parallel reporter assay, mSTARR-seq, could be used to simultaneously test for both enhancer-like activity and DNA methylation-dependent enhancer activity for millions of loci in a single experiment (Lea *et al*., 2018). Here we apply mSTARR-seq to query nearly the entire human genome, including almost all CpG sites profiled either on the commonly used Illumina Infinium MethylationEPIC array or via reduced representation bisulfite sequencing. We show that fragments containing these sites are enriched for regulatory capacity, and that methylation-dependent regulatory activity is in turn sensitive to the cellular environment. In particular, regulatory responses to interferon alpha (IFNA) stimulation are strongly attenuated by methyl marks, indicating widespread DNA methylation-environment interactions. In agreement, methylation-dependent responses to IFNA identified via mSTARR-seq predict methylation-dependent transcriptional responses to challenge with influenza virus in human macrophages. Our observations support the idea that pre-existing DNA methylation patterns can influence the response to subsequent environmental exposures—one of the tenets of biological embedding. However, we also find that, on average, sites previously associated with early life adversity are not more likely to functionally influence gene regulation than expected by chance.

Introduction

DNA methylation is sensitive to the environment, can remain stable across cell divisions, and in some contexts, can alter gene regulation. Consequently, it has received a high level of attention as a potential pathway linking environmental exposures to downstream trait variation, especially when these exposures are separated temporally, as proposed by the "biological embedding" hypothesis (Hertzman, 1999; Hertzman, 2012). In a canonical example, gestational manipulation of methyl donors in mice is causally implicated in changes in DNA methylation and expression levels of the *agouti* gene, which in turn affects susceptibility to obesity and insulin resistance later in life (Dolinoy *et al.*, 2006). However, the mechanism underlying the *agouti* case—"metastable" methylation of an inserted intracisternal A particle [IAP] class retrovirus—is now thought to be unusual (Kazachenka *et al.*, 2018). Thus, it remains unclear whether the many reports of environment-DNA methylation associations are likely to represent links along a causal pathway to phenotype, or are better viewed as passive biomarkers of exposure.

Experimental tests of the causal impact of DNA methylation on gene regulation indicate that both scenarios are possible. *In vitro* studies reveal that transcription factor binding is frequently (but not ubiquitously) sensitive to DNA methylation (O'Malley *et al.*, 2016; Yin *et al.*, 2017). More recently, epigenomic editing of DNA methylation marks has been shown to alter the activity of transcription factors important in disease and development *in vivo* (Greenberg and Bourc'his, 2019; Yim *et al.*, 2020), as well as the formation of CTCF-mediated gene loops (Lei *et al.*, 2017). However, other epigenetic editing studies show that, even within the same regulatory element, changes in DNA methylation have functional consequences for gene expression at only a subset of sites (e.g. Maeder *et al.*, 2013). Indeed, in the native genome, enhancer activity appears to be insensitive to DNA methylation levels in the majority of cases (Kreibich *et al.*, 2023). Time series analyses in human dendritic cells have also shown that, in response to a pathogen challenge, nearly all changes in gene expression precede changes in DNA methylation (Pacis *et al.*, 2019). Such methylation changes may nevertheless be functionally relevant if they influence the speed and magnitude of subsequent challenges (e.g., by marking the accessibility of latent enhancers across cell divisions) (Kamada *et al.*, 2018; Sun and Barreiro, 2020). This hypothesis may explain, for example, enhanced transcriptional responses to glucocorticoid stimulation in the descendants of hippocampal progenitor cells previously challenged with glucocorticoids (Provençal *et al.*, 2020).

Together, these findings suggest that environment-associated DNA methylation marks are mixed sets that include functionally silent sites, sites that are constitutively important for gene regulation, and sites in which DNA methylation levels affect gene regulation only under certain conditions. Disentangling which sites belong to which set is important for interpreting and prioritizing the results of a growing body of studies in the biological, social, and health sciences, especially those that test hypotheses that assume a functional role for DNA methylation, such as biological embedding (Hertzman, 2012; Demetriou *et al.*, 2015; Aristizabal *et al.*, 2020). To facilitate this process, we recently introduced a massively parallel reporter assay, mSTARR-seq, that is capable of testing the functional effects of DNA methylation on regulatory activity in high-throughput (Lea *et al.*, 2018). This method allowed us to test for methylation-dependent regulatory activity at millions of CpG sites in the human genome. However, our previous data set did not investigate how DNA methylation marks affect the response to environmental challenge. It also did not explicitly target the CpG sites that are the

most commonly assayed in the human genome (i.e., those featured on the Illumina MethylationEPIC array).

Here, we address these gaps by using mSTARR-seq to construct a genome-wide map of DNA methylation-dependent enhancer activity for 27.3 million CpG sites in the human genome, accomplished by assessing 600 bp windows encompassing 93.5% of CpGs in the human genome as a whole. This set includes 99.3% of CpG sites present on the Illumina MethylationEPIC array, the most commonly used platform for profiling DNA methylation in humans, and 99.4% of CpG sites accessible via reduced-representation bisulfite sequencing (RRBS; Meissner *et al.*, 2005). To evaluate the importance of DNA methylation in responses to environmental challenge, we performed mSTARR-seq under baseline conditions (i.e., no challenge) and following exposure to two physiologically relevant environmental challenges: dosage with the synthetic glucocorticoid dexamethasone, which plays a central role in metabolic regulation and stress-related homeostasis, and interferon alpha (IFNA), a cytokine that elicits genomic and immunological responses associated with viral infection.

We used these data to pursue three goals. First, we describe overall patterns of regulatory activity and methylation-dependent regulatory activity across profiled sites, including how sites targeted by the EPIC array or by RRBS compare to the genome as a whole. The results of this analysis produce a new resource: a map of DNA methylation-dependent enhancer activity across the human genome. Second, we test the degree to which methylation-dependent regulatory activity is affected by exposure to steroid hormone or immune defense-related signaling molecules. Our results yield insight into the frequency of DNA methylation-environment interactions genome-wide, and provide support for the hypothesis that DNA methylation potentiates the cellular response to external stressors. Finally, we illustrate the applicability of this resource by testing two predictions of the biological embedding hypothesis: that pre-existing DNA methylation levels can affect the transcriptional response to subsequent environmental challenge (Provençal *et al.*, 2020; Sun and Barreiro, 2020; Fanucchi *et al.*, 2021), and that sites linked to early life adversity (ELA) are likely to be functionally important for shaping gene expression. Our results suggest that mSTARR-seq can identify DNA methylation-environment interactions that also occur *in vivo* in human populations and can therefore help prioritize environment- and ELA-associated loci for future follow-up.

Results

mSTARR-seq captures enhancer activity and methylation-dependent enhancer activity genome-wide

We assessed regulatory activity and methylation-dependent regulatory activity for 4,558,475 600-base pair windows of the genome by pairing hybridization capture of targeted loci in the human genome with the massively parallel reporter assay, mSTARR-seq (Lea *et al.*, 2018). In brief, mSTARR-seq performs enzymatic manipulation of DNA methylation across hundreds of thousands to millions of reporter DNA fragments simultaneously. By measuring the ability of fragments to self-transcribe (as in Arnold *et al.*, 2013; Shlyueva *et al.*, 2014; reviewed in Gallego Romero and Lea, 2022), it generates estimates of the enhancer-like regulatory potential for each fragment when that fragment is in an unmethylated versus a methylated state (Figure 1A, B). Notably, results from the unmethylated condition are akin to those from a conventional STARR-seq experiment, in that they assess regulatory activity irrespective of CpG content or methylation status. To focus on the CpG sites most likely to be included in DNA

methylation studies in humans, we performed custom capture with SeqCap EZ Prime Choice Probes (Roche), targeting all CpG sites on the Illumina Infinium MethylationEPIC array and those likely to be profiled using reduced representation bisulfite sequencing, which enriches for CpG sites near targets of *MspI* restriction enzyme digestion (Figure 1-figure supplement 1). Because of substantial attention to potential environmental and early life effects on DNA methylation at the glucocorticoid receptor gene (*NR3C1*, reviewed in Liu and Nusslock, 2018), we also targeted the 6.5 Mb in and flanking *NR3C1*. Finally, to assess background expectations for regulatory and methylation-dependent regulatory activity in the human genome, we targeted a control set of 100,000 loci for capture, chosen at random across the human genome after excluding centromeres, gaps, and uncalled bases in the hg38 genome.

We generated an mSTARR-seq library from captured DNA from the GM12878 cell line, followed by transfection into the K562 erythroleukemic cell line and co-purification of plasmid-derived RNA and DNA (6 replicates per condition: methylated versus unmethylated; see Materials and Methods; Supplementary File 1). Based on our minimal criteria for assessment (600 basepair windows where at least half of the plasmid-derived DNA samples had non-zero reads covering the window; see Materials and Methods), 90.2% of the human genome was included in the plasmid DNA library purified at the end of the mSTARR-seq experiment (mean sequencing depth per replicate = 30.4 million reads; mean read coverage per window = 12.723 ± 41.696 s.d.). Within this set, which also included off-target regions, windows were ~15-fold enriched for targeted regions in the genome (Fisher's Exact Test $\log_2$(OR) [95% confidence interval (CI)] = 3.971 [3.934, 4.009], $p < 1.0 \times 10^{-300}$]). Thus, in windows that passed our minimal assessment criteria, we successfully targeted 99.3% of CpG sites on the MethylationEPIC array and 99.4% of sites likely to be included in RRBS libraries. Across target sets, read depth was not predicted by CpG density, indicating no systematic power differences in assessing methylation-dependent activity due to differences in CpG number per window (R^2 = 0.099, p = 0.6852; Supplementary file 2). Our results are comparable to published fragment diversity levels achieved with this method (Lea *et al*., 2018; Figure 1-figure supplement 2). Because demethylation or remethylation of DNA fragments could occur within cells during the experiment, we performed bisulfite sequencing at the end of the experiment. We confirmed that DNA methylation levels were substantially higher in the methylated condition samples than in the unmethylated samples, where methylation levels were near zero (mean methylated = 0.885, mean unmethylated = 0.066, Figure 1-figure supplement 3; unpaired t-test: t = -14.66, df = 15,124, $p = 2.39 \times 10^{-10}$). We note that the observed small deviations from 0% and 100% methylation would reduce our power to detect methylation-dependent activity, but should not incur false positive results.

To test for regulatory potential, we focused on those windows where at least 3 replicate samples produced non-zero RNA-seq reads in either the methylated condition or in the unmethylated condition (n = 216,091 non-overlapping 600 bp windows, 4.3% of the human genome; mean DNA-seq read coverage per window = 93.907 ± 10.091 s.d.; mean RNA-seq read coverage per window = 165.093 ± 1008.816). These inclusion criteria focused our analysis on the subset of windows where we were able to detect minimal evidence of transcription from the plasmid. The proportion of the human genome showing evidence of regulatory activity in STARR-seq family assays is expected to be small based on previous work. For example, Johnson and colleagues estimated that 0.165% of the human genome had regulatory potential in unstimulated A549 cells in a genome-wide STARR-seq assay, based on the proportion of hg38 basepairs that fell in regions with regulatory activity in their assay (Johnson *et al.*, 2018). Among

the regions analyzed here, 3,721 windows (1.7%) showed evidence for regulatory activity, where the amount of RNA generated from a window significantly exceeded the amount of DNA input sequenced for the same window (FDR < 1%; Supplementary File 3). Sequencing depth does not appear to constrain the ability to detect regulatory regions, as rarefaction analyses suggest that increasing sequencing depth of RNA or DNA libraries would add only a small number of additional regions with any evidence of transcriptional activity (Figure 1-figure supplement 4). Further, among analyzed windows, DNA coverage per fragment explains minimal variance in mSTARR-seq enhancer activity ($R^2 = 0.029$, $p < 1.0 \times 10^{-300}$).

Regions with regulatory activity were enriched for enhancers and active promoters annotated by the ENCODE Consortium for the K562 cell line ($\log_2(OR) = 0.584 – 3.337$; all $p < 1 \times 10^{-3}$; Figure 1C; Supplementary file 4 (ENCODE, 2012; Ernst and Kellis, 2012); note that previous research has found that promoters can show enhancer-like activity in STARR-seq-type assays (e.g. Klein *et al.*, 2020). In support of assay reproducibility, regulatory regions also were highly consistent with previous mSTARR-seq data generated in K562 cells using a previously published, independently generated DNA library that we reanalyzed using the current pipeline (overlap among windows with FDR < 1% in each data set analyzed independently: $\log_2(OR)$ [95% CI] = 6.212 [6.086, 6.440], $p < 1.0 \times 10^{-300}$; Figure 1-figure supplements 5-6; Supplementary Files 5-6) (Lea *et al.*, 2018).

Regions with mSTARR-seq-annotated regulatory activity also exhibited a high degree of consistency between cell types. In a comparison against newly generated mSTARR-seq data from the HepG2 liver cell line, using the same mSTARR-seq library as in the previously published K562 experiments (Lea *et al.*, 2018), regulatory regions detected in this study were enriched among regulatory regions detected in HepG2 cells ($\log_2(OR)$ [95% CI] = 3.534 [3.381, 3.684], $p = 5.21 \times 10^{-307}$; Figure 1-figure supplements 5 and 7; Supplementary File 7). They also overlap with regulatory regions identified in a conventional STARR-seq experiment in A549 lung epithelial cells ($\log_2(OR)$ [95% CI] = 2.451 [2.442, 2.461], $p < 1.0 \times 10^{-300}$) (Johnson *et al.*, 2018). Although we prioritized a blood-derived cell line because of the frequency of environmental epigenetic studies done in blood, these results suggest that our findings can be generalized, to some extent, to other cell and tissue types.

Among the 3,721 windows with regulatory activity in either the methylated or unmethylated condition, 1,768 windows (47.5% of regulatory windows; FDR < 1%) were differentially active depending on condition, pointing to DNA methylation-dependent regulatory activity. This result is also concordant when we apply the current pipeline to previously published data from K562s and our new HepG2 data, which exhibit correlated effects of DNA methylation on regulatory activity in the windows examined in both cases (K562: $R^2 = 0.286$ for 1250 regulatory windows with FDR < 1% in both data sets, $p = 3.19 \times 10^{-93}$; HepG2: $R^2 = 0.277$ for 511 regulatory windows with FDR < 1% in both data sets, $p = 8.87 \times 10^{-38}$ Figure 1-figure supplement 8). Among methylation-dependent regulatory regions, the majority of regions (1744 windows, 98.6%) were more active in the unmethylated condition than the methylated condition (Figure 1-figure supplements 9, 10). Consistent with previous findings (Lea *et al.*, 2018), regulatory regions with more CpGs are more likely to be repressed by DNA methylation (Figure 1-figure supplement 11; Spearman's rho = 0.370, $p = 9.865 \times 10^{-121}$; n = 3,721 regions with mSTARR-seq regulatory activity). Regulatory windows showing higher activity in the methylated condition (24 windows) were enriched for binding motifs of the transcription factors p53, which has been previously reported to have increased binding affinity to methylated DNA relative to unmethylated DNA (Kribelbauer *et al.*, 2017) ($\log_2(OR)$ [95% CI] = 2.352 [0.714,

3.767], p = 2.91 x 10^{-3}; Supplementary File 8), and Tfcp2I1, which has been found to recruit Tet2 to mediate enhancer demethylation (Sardina *et al.*, 2018) ($\log_2$(OR) [95% CI] = 2.615 [0.580, 4.229], p = 6.84 x 10^{-3}).

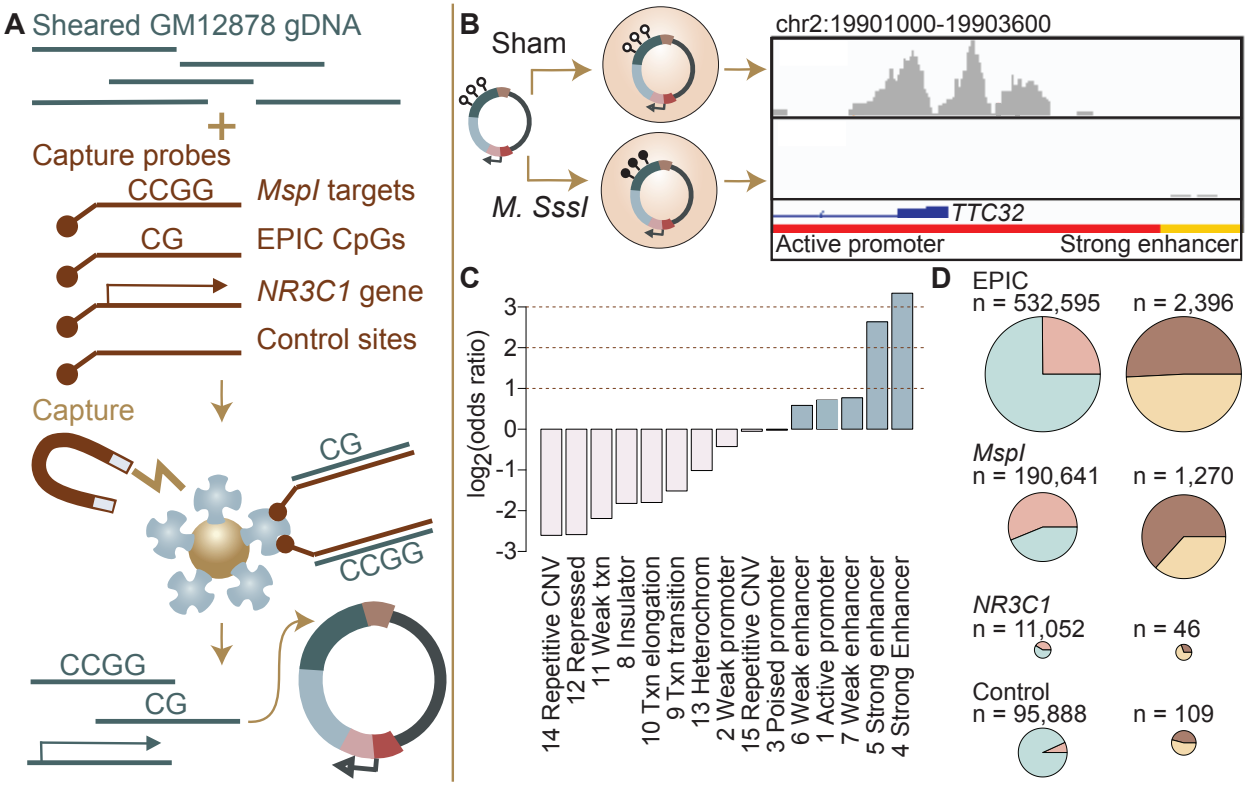

Figure 1. Study design and identification of enhancer activity. (A) Sheared DNA from the GM12878 cell line was subjected to enrichment via capture with probes targeting loci selected in reduced representation bisulfite sequencing (RRBS) workflows (*MspI* targets), CpG sites on the Infinium EPIC array, the gene *NR3C1* and flanking regions, and 100,000 randomly distributed control regions. Note that a single 600 bp window can contain multiple target types (Figure 1-figure supplement 1). Library diversity summaries are shown in Figure 1-figure supplement 2. **(B)** Captured loci were cloned into the mSTARR-seq vector, *pmSTARRseq1*, treated with either the CpG methylating enzyme *M. SssI* or a sham treatment, and transfected into K562 cells. Methylation levels post-transfection and rarefaction analyses of sequencing depth of replicate samples are shown in Figure 1-figure supplements 3, 4. Right panel shows an example of DNA methylation-dependent regulatory activity near the first exon of the *TTC32* gene, where the methylation-dependent regulatory element overlaps an active promoter chromatin state (red horizontal bar denotes active promoter as defined by ENCODE: ENCODE, 2012). **(C)** mSTARR-seq regulatory activity in the baseline condition is strongly enriched in ENCODE-defined enhancers and some classes of promoters (indicated in blue), and depleted in repressed, repetitive, and heterochromatin states. See Supplementary file 4 for full results of this analysis. Regions with mSTARR-seq regulatory activity detected in this experiment also significantly overlap with regions with regulatory activity in other mSTARR-seq and conventional STARR-seq datasets (Figure 1-figure supplement 5; see also Figure 1-figure supplement 6 for estimates of concordance across technical replicates). **(D)** Left column shows, under the baseline condition (i.e. unstimulated cells), the proportion of 600 bp windows that exhibited minimal regulatory activity (at least 3 replicate samples produced non-zero RNA-seq reads in either the methylated condition or the unmethylated condition) in the mSTARR-seq assay (pink) versus those with detectable input DNA but no evidence of regulatory activity (blue), for windows containing sites from each target set. Right column shows the proportion of windows with regulatory capacity (i.e., the subset of the windows represented in pink on the left that produce excess RNA relative to the DNA input at FDR

< 1%) that are also methylation-dependent (dark brown). Within each column, pie charts are scaled by the total numbers of windows represented. See Figure 1-figure supplements 7 and 8 for comparisons to regulatory regions in other datasets. Figure 1-figure supplements 9 and 10 show window-level RNA to DNA ratios. Figure 1-figure supplement 11 shows the relationship between CpG density and methylation-dependent regulatory activity.

Commonly studied CpG sites are enriched for methylation-dependent regulatory activity

We compared methylation-dependent regulatory activity between CpGs targeted on the EPIC array, CpGs typically profiled in RRBS libraries (i.e., near *MspI* cut sites), the 6.5 Mb in or flanking the glucocorticoid receptor gene *NR3C1*, and the control set of genome-representative loci. As expected, windows that contained EPIC CpG sites, sites associated with RRBS, or that were located in or near *NR3C1* were significantly more likely to show at least some degree of transcriptional activity (i.e., show plasmid-derived RNA reads in at least half the sham or methylated replicates) than the genomic background (i.e., 98,967 randomly distributed loci: see Materials and Methods), and thus were more likely to be included in our analysis set (n = 216,091 windows) for regulatory activity (EPIC: $\log_2$(OR) [95% CI] = 2.189 [2.152, 2.227], $p < 1.0 \times 10^{-300}$; RRBS: $\log_2$(OR) [95% CI] = 4.126 [4.086, 4.163], $p < 1.0 \times 10^{-300}$; *NR3C1*: $\log_2$(OR) [95% CI] = 3.259 [3.193, 3.325], $p < 1.0 \times 10^{-300}$; Figure 1D). However, conditional on minimal transcriptional activity, windows containing EPIC array sites were not more likely to exhibit *significant* enhancer-like regulatory activity (FDR < 1%; n = 3,721 windows) than background windows of the genome, and RRBS- and *NR3C1*-associated sites were in fact slightly less likely to do so (EPIC: $\log_2$(OR) [95% CI] = 0.112 [-0.168, 0.405], p = 0.47; RRBS: $\log_2$(OR) [95% CI] = -0.493 [-0.779, -0.195], $p = 1.11 \times 10^{-3}$; *NR3C1*: $\log_2$(OR) [95% CI] = -0.730 [-1.263, -0.217], $p = 3.89 \times 10^{-3}$). This result is likely explained by our inclusion criteria, as only regions with evidence for minimal RNA transcription were retained prior to formal analysis.

In contrast, among regions with detectable regulatory activity, 63.3% of those containing RRBS-associated CpG sites exhibited methylation-dependent regulatory activity, compared to 45.9% of control background loci (RRBS against control: $\log_2$(OR) [95% CI] = 1.025 [0.430, 1.624], $p = 4.39 \times 10^{-4}$; Figure 1D). Note that of 109 regulatory windows in the control set, 108 contain at least 1 CpG, so this difference is not because the control set is CpG-free (mean number CpGs per fragment in control set = 13.291 ± 11.179 s.d.; EPIC = 19.641 ± 14.471; RRBS = 20.870 ± 13.883; *NR3C1* = 7.405 ± 9.409). Neither windows with EPIC CpGs nor windows in or near *NR3C1* were enriched for methylation-dependent regulatory activity relative to the genomic background (EPIC against control: $\log_2$(OR) [95% CI] = 0.284 [-0.297, 0.871], p = 0.33; *NR3C1* versus control: $\log_2$(OR) [95% CI] = -0.948 [-2.129, 0.178], p = 0.11). Consequently, differential methylation identified through RRBS is more likely to be capable of driving differences in gene regulation, as detectable by mSTARR-seq, than differential methylation elsewhere in the genome. We caution, however, that even among RRBS sites, 98.8% do not occur in regions of the genome with detectable regulatory activity in either the methylated or unmethylated conditions, at least in the K562 cell type, and 35.0% of those that fall in putative regulatory elements exhibit no evidence for methylation-dependent activity.

Environmental perturbation reveals cryptic regulatory elements and cryptic effects of DNA methylation

Enhancer activity can be cell type- or environment-dependent (e.g., Ostuni *et al.*, 2013; Johnson *et al.*, 2018; Chaudhri *et al.*, 2020). DNA methylation-dependent enhancer activity may

296 show similar context-dependence, thus potentially accounting for the large number of sites that
297 fall in functionally silent regions described above. However, this possibility has not been
298 systematically tested. To do so, we next compared regulatory activity between the baseline
299 unchallenged condition and cells challenged with interferon alpha (IFNA) or dexamethasone
300 (dex) (Figure 2A; Figure 2-figure supplements 1-2; Supplementary file 9). Regions that were
301 identified to have regulatory potential in the baseline condition were highly likely to retain
302 regulatory potential after cells were challenged with IFNA or dex (Figure 2-figure supplement 3;
303 IFNA $\log_2$(OR) [95% CI] = 8.639 [8.499, 8.812], $p < 1.0 \times 10^{-300}$; dex $\log_2$(OR) [95% CI] =
304 9.640 [9.483, 9.776], $p < 1.0 \times 10^{-323}$; Supplementary Files 10-11). However, environmental
305 challenges also revealed thousands of putative regulatory regions that were undetectable at
306 baseline but active post-stimulation (Figure 2B; 1614 IFNA-specific; 1131 dex-specific). Of
307 4,632 IFNA regulatory regions (<1% FDR), 44.1% are not detectable at baseline at a 1% FDR
308 threshold in the baseline condition, and even with a relaxed baseline FDR of 10%, 25.1% remain
309 undetectable. Of 4,217 dex regulatory regions (<1% FDR), 40.2% are not detectable at baseline
310 (1% FDR), and 31.5% remain undetectable at a baseline FDR of 10%.
311 Regulatory windows specific to the IFNA treatment were enriched for 33 transcription
312 factor binding motifs (TFBMs) (Supplementary File 12), with strong enrichments detected for
313 TFBMs involved in innate immune defense in general, and interferon signaling specifically
314 (Figure 2C). For example, the most enriched motif was the canonical DNA target of interferon
315 signaling, known as IFN-stimulated response elements (ISRE; $\log_2$(OR) [95% CI] = 3.158
316 [2.953, 3.358], Bonferroni corrected $p = 7.31 \times 10^{-133}$), followed by binding motifs for several
317 IFN-regulatory factors (IRF1, IRF2, IRF3, IRF4, IRF8; all OR > 1.5 and Bonferroni corrected p
318 $< 1 \times 10^{-15}$) (Chen *et al.*, 2017). Regulatory windows specific to the dex-stimulated condition
319 were significantly enriched for 28 transcription factor binding motifs, including the
320 glucocorticoid response element IR3 and binding motifs of several transcription factors known to
321 interact with or be modulated by the glucocorticoid receptor (AP-1, CEBP:CEBP, CEBP:AP1,
322 JunB, Jun-AP1, GATA1, STAT3, and STAT5; all OR > 1.3, Bonferroni corrected $p < 0.01$;
323 Supplementary File 13) (Cain and Cidlowski, 2017). Results were qualitatively similar if we
324 used a more stringent definition of IFNA-specific and dex-specific regulatory activity (e.g.
325 "IFNA-specific" defined as FDR < 1% in IFNA condition and FDR > 10% in the other two
326 conditions; Supplementary Files 14-15).
327 To evaluate the relevance of these regions to *in vivo* gene regulation, we also generated
328 matched mRNA-seq data for the endogenous K562 genome from the same experiments. These
329 data showed that expressed genes located closest to mSTARR-seq-annotated, IFNA-specific
330 enhancers were more strongly upregulated after IFNA stimulation than the set of expressed
331 genes located closest to shared mSTARR-seq-annotated enhancers (i.e., those identified in both
332 the IFNA and at least one other condition, considering genes within 100 kb maximum distance
333 from each enhancer element; unpaired t-test; $t = 3.268$, $df = 601.88$, $p = 1.15 \times 10^{-3}$). We found
334 similar results when using inferred enhancer-gene linkages from the EnhancerAtlas 2.0 (Gao *et*
335 *al.*, 2016) and restricting the set of IFNA-specific enhancers to those with external experimental
336 support for ISRE binding (n = 1005 windows; ChIP-Seq data from ENCODE [2012], relative to
337 all other genes in the gene expression dataset; unpaired t-test; $t = 3.579$, $df = 118.36$, $p = 5.01 \times$
338 10^{-4}; Figure 2D; Supplementary File 16). Despite a weaker overall gene expression response to
339 dex, genes closest to dex-specific mSTARR-seq enhancers were also more strongly upregulated
340 after dex stimulation than genes near shared enhancers (unpaired t-test; $t = 3.477$, $df = 479.6$, $p =$
341 5.53×10^{-4}).

342 For the IFNA challenge, the DNA methylation state of each window appears to play an
343 important role in shaping condition-specific responses to stimulation in the mSTARR-seq data
344 set. Nearly twice as many regulatory windows (81.4%; 1314 of 1614) exhibited methylation-
345 dependent regulatory activity in the IFNA-specific condition than in the baseline or dex-specific
346 condition (47.5% and 48.4% respectively; two-sided binomial test for IFNA compared to
347 baseline: $p = 3.58 \times 10^{-312}$). Further, regulatory regions that harbor TFBMs for TFs central to the
348 interferon response (ISRE, IRF1, IRF2, IRF3, IRF4, IRF8; N = 663 windows) strongly
349 responded to IFNA challenge if in an unmethylated state, but mounted systematically attenuated
350 responses if in a methylated state. As a result, 562 of these 663 windows (84.7%) exhibited
351 significant methylation-dependent regulatory activity and 561 of them (99.8%) were more active
352 in the IFN-challenged state when unmethylated. This pattern is recapitulated when focusing on
353 analyzed windows with external experimental support for ISRE binding (n = 1005 windows;
354 ChIP-Seq data from ENCODE [2012]). These windows show no evidence for methylation-
355 dependent regulatory activity in the baseline condition (paired t-test; $t = -0.792$, $df = 1004$, $p =$
356 0.43), primarily because they show no regulatory activity at all without IFNA stimulation. After
357 IFNA stimulation, though, they exhibit strong methylation-dependence. Specifically, only
358 unmethylated windows are capable of a response (paired t-test; $t = 31.748$, $df = 1004$, $p = 1.02 \times$
359 10^{-153}; Figure 2E).

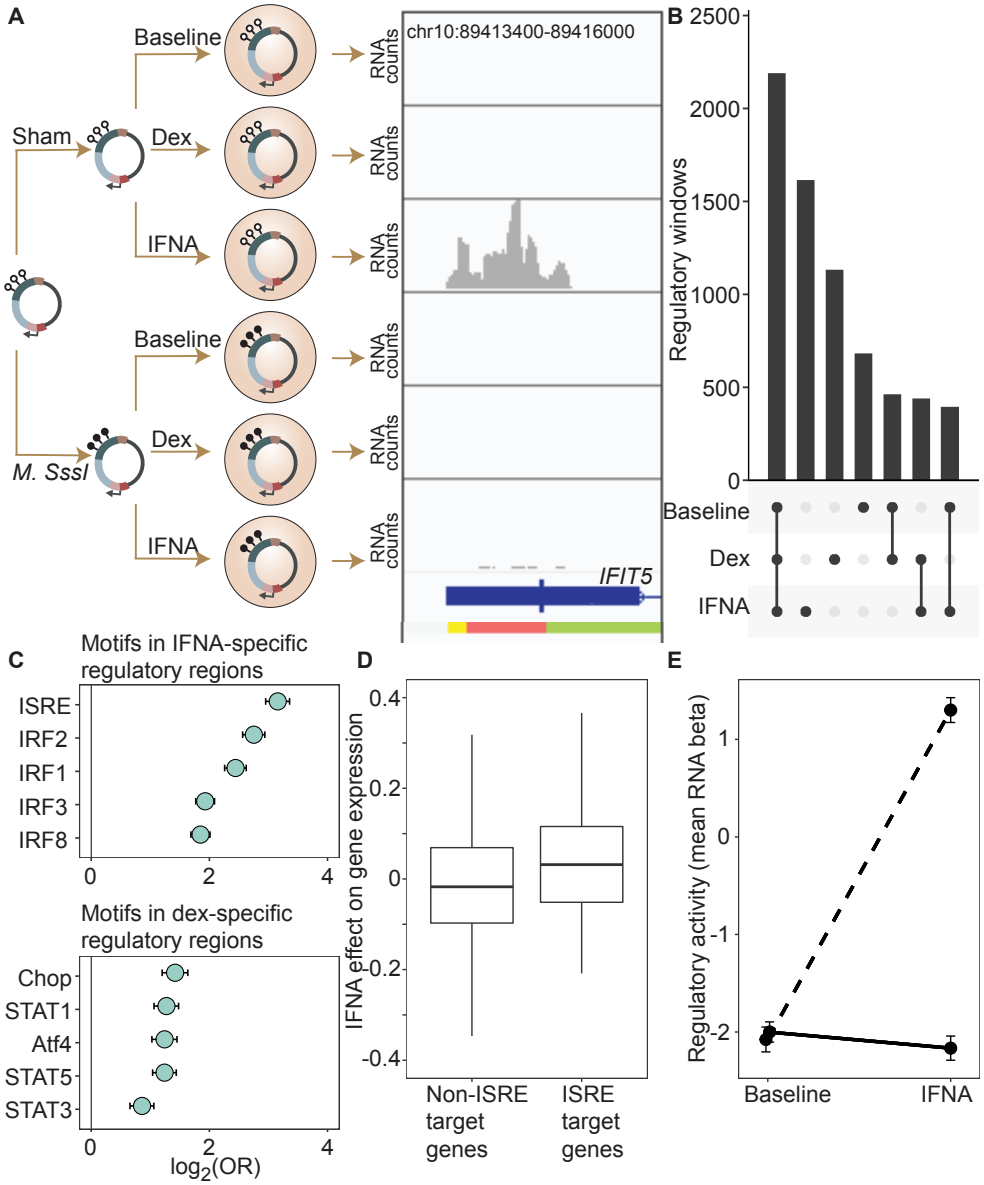

Figure 2. DNA methylation-environment interactions reveal methylation-dependent responses to IFNA and dexamethasone challenge. (A) Full mSTARR-seq design across DNA methylation and challenge conditions (see Figure 2-figure supplements 1 and 2 for filtering and overlap of the datasets, and Supplementary Files 3, 10, and 11 for effect sizes). An example of a DNA methylation-environment interaction is shown overlapping the interferon-induced gene *IFIT5* and an ENCODE-annotated weak promoter (pink denotes weak promoter, yellow denotes heterochromatin, and green denotes weak transcription; the endogenous *IFIT5* gene expression response to IFNA in our experiment is shown in Figure 2-figure supplement 4). Three consecutive 600 bp windows have interaction FDR < 1 x 10^{-4} in this region. Panels depict non-normalized, raw read pileups for mSTARR-seq RNA replicates, with all y-axis maximums set to 14000. No methylation-dependent activity is detectable in the baseline condition because this enhancer element is inactive. Upon IFNA stimulation, only unmethylated enhancer elements are capable of responding. **(B)** Upset plot showing shared and unique mSTARR-seq identified enhancer elements across conditions. While many elements are shared, 3426 are unique to a single condition (FET log-odds results for magnitude of overlap are shown in Figure 2-figure supplement 3). **(C)** Top five most enriched transcription factor binding motifs in IFNA- and dex-specific mSTARR-seq enhancers, compared to all windows tested. Whiskers show the 95% CI. See Supplementary Files 12 and 13 for all

enrichment results. **(D)** Genes targeted by ISRE enhancers (ISRE enhancers identified from ENCODE ChIP-seq data; gene targets identified from enhancer-gene linkages from EnhancerAtlas 2.0: Gao *et al.*, 2016) that are also identified as IFNA condition-specific mSTARR-seq enhancers show stronger K562 endogenous gene expression responses to IFNA stimulation than non-ISRE targets (unpaired t-test: $t = 3.58$, $df = 118.36$, $p = 5.01 \times 10^{-4}$; Supplementary File 16). Each box represents the interquartile range, with the median value depicted as a horizontal bar. Whiskers extend to the most extreme values within 1.5x of the interquartile range. **E)** mSTARR-seq regulatory activity for windows containing ISRE targets (n = 1005 windows) interacts strongly with exposure to IFNA. These windows are capable of mounting a strong response to IFNA stimulation when unmethylated (dashed line; paired t-test: $t = 23.02$, $df = 1004$, $p = 1.78 \times 10^{-94}$) but not when methylated (solid line; paired t-test: $t = -1.74$, $df = 1004$, $p = 0.082$). Dots show the mean beta corresponding to enrichment of RNA reads versus DNA reads across windows; whiskers show the standard error. Because y-axis values correspond to model estimates, they can be positive (i.e., more mSTARR-seq RNA reads than input DNA reads) or negative values (i.e., fewer mSTARR-seq RNA reads than mSTARR-Seq input DNA reads, indicating no regulatory activity).

Methylation levels at mSTARR-seq IFNA-specific enhancers predict the transcriptional response to influenza virus in human macrophages

Our findings show that, in the context of mSTARR-seq, pre-existing DNA methylation state can capacitate or constrain the regulatory response to IFNA stimulation. This result suggests that DNA methylation-environment interactions may be an important determinant of gene expression levels *in vivo*. To test this possibility, we drew on matched whole genome bisulfite sequencing (WGBS) and RNA-seq data collected from human monocyte-derived macrophages (n = 35 donors), with and without infection with the influenza A virus (IAV), commonly known as flu (Figure 3A; Aracena *et al.*, in press). We asked whether variation in the gene expression response to flu is predicted by DNA methylation levels in the baseline (non-infected) condition, especially at loci where the response to IFNA is affected by DNA methylation in mSTARR-seq. Importantly, flu and IFNA challenges induce similar innate immune responses (Killip *et al.*, 2015).

Within each individual in the macrophage data set, mean DNA methylation levels at baseline significantly predict the mean gene expression response to flu across the full set of mSTARR-seq enhancer windows detected in the IFNA condition: higher methylation at baseline predicts an attenuated gene expression response, on average (n = 35 individuals at 2769 enhancer windows: mean Pearson's $r = -0.105 \pm 0.006$ s.d., all Bonferroni-corrected $p < 3 \times 10^{-5}$; Supplementary File 17). This effect is largely driven by the subset of mSTARR-seq IFNA-specific enhancers. Specifically, the correlation between baseline DNA methylation levels and the gene expression response to flu is 3.44-fold stronger in IFNA-specific enhancers than for enhancers identified in both the IFNA condition and at least one other condition (Figure 3B; IFNA-specific enhancers: n = 1033, mean Pearson's $r = -0.170 \pm 0.009$ s.d., all Bonferroni-corrected $p < 2 \times 10^{-5}$; shared enhancers: n = 1736, mean Pearson's $r = -0.049 \pm 0.01$ s.d., all Bonferroni-corrected $p > 0.1$). These results appear to be driven by strong methylation-dependence in flu-infected cells, as the average within-individual correlation between DNA methylation and gene expression is 2.44 times as large after infection ($r = -0.261 \pm 0.006$) than at baseline ($r = -0.106 \pm 0.008$) in IFNA-specific mSTARR-seq enhancers (Figure 3C; Supplementary File 18).

The limited sample size of the macrophage data set makes it better suited for analyses of the overall relationship between DNA methylation and gene expression within an individual, rather than locus-specific analyses of interindividual variation (especially as locus-specific

423 variance in DNA methylation across individuals is low: mean = 0.004, standard deviation =
424 0.008). Nevertheless, across 1382 testable loci (600 bp windows containing at least 1 CpG with
425 interindividual variance > 0.01), we identified one IFNA-specific, methylation-dependent
426 mSTARR-seq enhancer where endogenous variation in DNA methylation levels across
427 individuals clearly predicts the response of the nearest gene's transcriptional response to flu
428 (Figure 3D-E; $p = 6.05 \times 10^{-5}$, q-value = 0.0837; Supplementary File 19). This mSTARR-seq
429 enhancer (chr1:1013400-1014000) overlaps the promoter of interferon-stimulated gene 15
430 (*ISG15*; Figure 3E), and its average methylation explains 38% of the variance in the *ISG15*
431 transcriptional response to flu across individuals. The magnitude of *ISG15* transcriptional
432 response to flu appears primarily driven by the enhancer's effect on gene expression at baseline.
433 Lower enhancer methylation at baseline is associated with higher *ISG15* expression at baseline,
434 ultimately resulting in a shallower fold change response to flu (Figure 3-figure supplement 1).
435 This example illustrates the value of integrating observational data on DNA methylation and
436 gene expression with mSTARR-seq. The population data support the *in vivo* relevance of the
437 mSTARR-seq data, while the mSTARR-seq data suggest that baseline variation in *ISG15*
438 methylation *in vivo* is causally meaningful to the response to influenza. Notably, *ISG15* plays
439 critical roles in regulating the type I interferon response and modulating host immunity to both
440 viral and bacterial infections (reviewed in Perng and Lenschow, 2018).

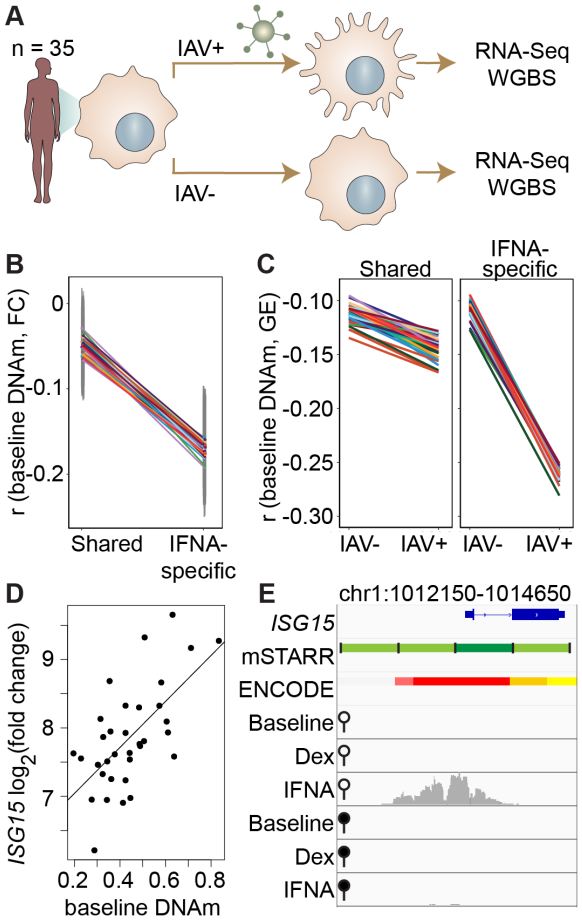

441 **Figure 3. DNA methylation in mSTARR-seq enhancers predicts *in vivo* gene expression in**
442 **macrophages. (A)** Study design of the in *vivo* experiment, in which matched macrophage samples from
443 35 individuals were either left non-infected or infected with influenza A virus (IAV) for 24 hours and

444 processed for RNA-seq and whole genome bisulfite sequencing (WGBS; Aracena *et al.*, in press). **(B)**
445 Within individuals, DNA methylation (DNAm) levels at mSTARR-seq enhancers in non-infected cells
446 are negatively correlated with the nearest genes' transcriptional responses to IAV, but only in mSTARR-
447 seq enhancers that were specific to the IFNA condition (IFNA-specific enhancers: n = 1033, mean
448 Pearson's r = -0.170 ± 0.009 s.d., all Bonferroni-corrected $p < 2 \times 10^{-5}$; shared enhancers: n = 1736, mean
449 Pearson's r = -0.049 ± 0.01 s.d., all Bonferroni-corrected p > 0.1). Each colored line represents an
450 individual, and vertical gray lines represent 95% confidence intervals (see Supplementary File 17 for full
451 results). **(C)** The average within-individual correlation (r) between DNA methylation and gene expression
452 (GE) is 2.44 times as large after infection (r = -0.261 ± 0.006) than at baseline (r = -0.106 ± 0.008) in
453 IFNA-specific mSTARR-seq enhancers (right panel), but much less affected by infection at mSTARR-
454 seq enhancers that are shared across conditions (left panel). Within each panel, each colored line
455 represents an individual for the same set of enhancers (see Supplementary File 18 for full results), without
456 and with IAV infection. **(D)** Across individuals, the *ISG15* transcriptional response to IAV is significantly
457 correlated with average DNAm at the mSTARR-seq enhancer chr1:1013400-1014000 in non-infected
458 cells ($R^2 = 0.381$, $p = 6.05 \times 10^{-5}$, q = 0.084). Each dot represents an individual (see Supplementary File
459 19 for full results and Figure 3-figure supplement 1 for condition-specific results). **(E)** The mSTARR-seq
460 enhancer predictive of *ISG15* response to IAV (dark green bar) is located in the active promoter of *ISG15*
461 (as defined by ENCODE [ENCODE, 2012]; red denotes active promoter, pink denotes weak promoter,
462 orange denotes strong enhancer, yellow denotes weak enhancer). Three adjacent, methylation-dependent,
463 IFNA-specific mSTARR-seq enhancers were identified (light green), but do not significantly predict
464 *ISG15* response to IAV (q > 10%). The bottom 6 tracks depict non-normalized, raw read pileups for
465 mSTARR-seq RNA replicates in either the unmethylated (open circle) or methylated (filled circle)
466 condition, with all y-axis maximums set to 20,000.
467
468 **Most CpG sites associated with early life adversity do not show regulatory activity in K562s**
469 Finally, because changes in DNA methylation are of particular interest to research on the
470 biological embedding of early life experience (Hertzman and Boyce, 2010), we tested whether
471 DNA methylation differences associated with early life adversity (ELA) translate to functional
472 effects on gene regulation in the mSTARR-seq data. We first performed a literature search to
473 compile CpG sites that have previously been associated with ELA in humans using the Illumina
474 EPIC array or one of its precursors (Infinium Human Methylation 450K and 27K BeadChips).
475 Our search resulted in a total of 27 studies (Supplementary File 20), which together identified
476 8,525 unique ELA-associated sites.
477 For 26 of 27 studies, ELA-associated CpG sites were not more likely to occur within
478 putative regulatory windows (detected in either the methylated condition, unmethylated
479 condition, or both) than background chance (Figure 4). This pattern was qualitatively consistent
480 regardless of whether we considered baseline, IFNA-, or dex-challenged samples
481 (Supplementary File 20). The only exception was for a set of differentially methylated regions in
482 the children of mothers exposed to objective hardship (e.g., living in a shelter, loss of electricity)
483 who were pregnant during or within 3 months of the 1998 Quebec Ice Storm (Cao-Lei *et al.*,
484 2014). In this study, ELA-associated sites were more likely to fall in windows with regulatory
485 potential in our sample ($\log_2$(OR) [95% CI] = 1.343 [0.715, 1.909], $p = 3.39 \times 10^{-5}$). Among
486 these sites, 53.85% were also detected to have methylation-dependent activity, which is slightly,
487 but not significantly higher than the proportion of methylation-dependent sites on the Illumina
488 Methylation450K chip as a whole ($\log_2$(OR) [95% CI] = 0.884 [-0.338, 2.130], p = 0.16).
489 Consequently, ELA-associated sites in this study were not more likely to exhibit methylation-
490 dependent activity than chance. We speculate that regulatory enrichment in this data set is due to
491 its focus on intermediately methylated CpG sites with substantial interindividual variance in

492 DNA methylation levels, which tends to enrich for enhancer elements. Indeed, ELA-associated
493 sites in this study were more strongly enriched in enhancer regions than the union set of sites in
494 other studies we investigated ($\log_2$(OR) [95% CI] = 1.295 [0.543, 2.015], p = 6.64 x 10^{-4}).

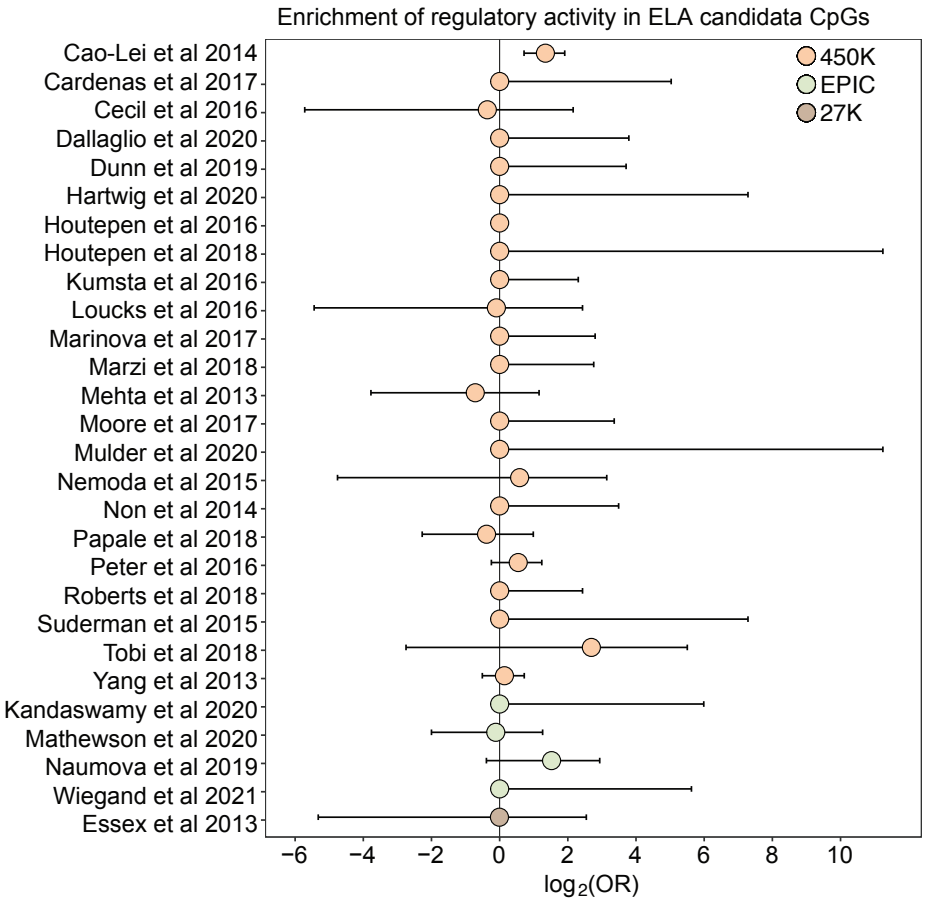

495 **Figure 4. Early life adversity-associated CpG sites are not enriched for mSTARR-seq regulatory**
496 **activity.** Log_2-tranformed odds ratios from Fisher's Exact Tests for enrichment relative to the background
497 set of sites on each array platform, for 27 studies of early life adversity-DNA methylation level
498 correlations (see Supplementary File 20 for full FET results). Whiskers show standard error. Only Cao-
499 Lei *et al*., 2014 shows significant enrichment for regulatory activity ($\log_2$(OR) [95% CI] = 1.343 [0.715,
500 1.909], p = 3.39 x 10^{-5}), but these sites are not more likely to exhibit methylation-dependent activity than
501 expected by chance ($\log_2$(OR) [95% CI] = 0.884 [-0.338, 2.130], p = 0.16). For details on the source
502 tissue and measures of ELA, see Figure 4-figure supplement 1.
503
504 **Discussion**
505 Using mSTARR-seq, we assessed the functional role of DNA methylation across more
506 than 99% of CpG sites assessed by two commonly used methods to measure methylation (the
507 EPIC array and RRBS). Compared to our previous work, we identify a higher rate of
508 methylation-dependence in the present data set (47.5% of analyzed windows in the current data
509 set versus 10% of analyzed windows from Lea *et al.* (2018) when we apply the current pipeline
510 to analyze both datasets; Supplementary Files 3, 6). This difference likely stems from lower
511 variance between replicates in the present study, which increases power (Figure 1-figure

512 supplement 6). Thus, our findings reveal that DNA methylation often significantly attenuates
513 regulatory activity in K562 enhancer and promoter elements.
514 The results also support the idea that CpG sites identified by environment-DNA
515 methylation association are a mixed bag. For example, despite the pervasive assumption in the
516 literature and in popular science that early adversity causally impacts downstream outcomes
517 through persistent epigenetic modification (e.g., Dubois *et al.*, 2019), 98% of CpG sites
518 associated with early life adversity in the literature fell in windows with no discernable
519 regulatory potential in K562 cells, irrespective of their methylation status or cellular state. Our
520 findings suggest that many ELA-associated sites may be better treated as passive biomarkers of
521 exposure rather than links on the causal pathway between early life disadvantage and later life
522 health outcomes. However, other cell types and cellular contexts should be tested to further
523 evaluate this hypothesis (we used the erythroleukemic K562 cell line, as ELA-associated sites
524 are most commonly assessed in blood). For instance, while we included the dexamethasone
525 condition here because glucocorticoid dysregulation is commonly invoked in association with
526 the response to early life adversity, the relationship between glucocorticoid signaling and early
527 life adversity is complex (Eisenberger and Cole, 2012; Koss and Gunnar, 2018) and may not be
528 well-modeled by acute glucocorticoid exposure. Given that the repertoire of poised and active
529 enhancers often differs across cell types and cellular states, expanding experimental approaches
530 like mSTARR-seq to other contexts can therefore serve a valuable role in prioritizing CpG sites
531 identified in observational studies of differential methylation (e.g., CpG sites associated with
532 disease).
533 Our results dovetail with work supporting the importance of CpG sites within enhancer
534 elements in responding to environmental perturbations (Pacis *et al.*, 2015; Husquin *et al.*, 2018).
535 Indeed, one of the most interesting findings from our analysis is the observation that DNA
536 methylation-environment interactions are widespread in the human genome. Across thousands of
537 genomic regions, both regulatory activity and methylation-dependent effects on regulatory
538 activity were only detectable upon stimulation, consistent with a model in which DNA
539 methylation contributes to epigenomic priming by modulating responsivity to environmental
540 stimuli (Kamada *et al.*, 2018; Sun and Barreiro, 2020). In support of this idea, IFNA-specific
541 enhancers detected in mSTARR-seq are able to nonrandomly identify collections of loci in the
542 genome where baseline DNA methylation also predicts the endogenous gene expression
543 response to flu infection (Figure 3B-C). This relationship is easier to discern in within-individual
544 comparisons across loci than in locus-by-locus analyses of interindividual variation. However,
545 we were also able to pinpoint one specific gene, *ISG15*, in which baseline DNA methylation
546 explains a large fraction of population variation in the gene expression response to flu (Figure
547 3D-E). Notably, the effect size for *ISG15* is very large, accounting for over a third of total
548 variance in the fold-change gene expression response to flu. Unfortunately, a comparable *in vivo*
549 dataset for dex challenge was unavailable to conduct parallel validation studies. However, our
550 results overall suggest that mSTARR-seq could help identify additional *in vivo* DNA
551 methylation-environment interactions, given sufficiently large sample sizes and data on the
552 environmental exposures of interest.
553 Applying mSTARR-seq in additional cell types may therefore help resolve whether DNA
554 methylation is responsible for exaggerated transcriptional responses to repeated challenges, as
555 previously suggested for glucocorticoid exposure in hippocampal progenitor cells (Provençal *et*
556 *al.*, 2020), or whether differential methylation after pathogen infection contributes to the
557 emerging paradigm of "trained immunity" in innate immune cells (reviewed in Fanucchi *et al.*,

558 2021). More generally, while our findings agree with the idea that many differences in DNA
559 methylation—even extreme ones (~0% versus ~100%) like those tested here—are silent with
560 respect to transcription factor binding and gene expression (e.g., Maeder *et al.*, 2013; Kreibich *et*
561 *al.*, 2023), they also suggest that the functional importance of DNA methylation is likely to be
562 underestimated without considering its interaction with the cellular environment.
563
564 **Materials and Methods**
565 *DNA capture and mSTARR-seq*
566 We used the DNEasy Blood and Tissue Kit (Qiagen) to extract 5 ug DNA from the
567 GM12878 lymphoblastoid cell line. We sheared the extracted DNA on a Covaris S2 with the
568 following parameters: intensity=3; duty cycle=5%, cycles/burst=200, treatment time=40 seconds,
569 temperature=4° C; intensifier=yes. We then performed agarose gel size selection of ~600-700 bp
570 DNA fragments followed by purification with the Qiaquick Gel Extraction Kit (Qiagen). We
571 note that we intentionally targeted longer fragments (~600-700 bp) than those targeted in (Lea *et*
572 *al.*, 2018) (~300-700 bp) because our previous work showed that longer fragments are more
573 likely to drive regulatory activity (Lea *et al.*, 2018).
574 We used Roche's NimbleDesign Software to design probes to capture the following
575 genomic regions: (i) EPIC CpGs targeted by the Illumina Infinium MethylationEPIC microarray
576 (862,831 CpGs); (ii) predicted CpG cut sites from an *in silico Msp1* digest of the hg38 genome,
577 followed by *in silico* size selection to 100-500 bp, which together simulates the first step in
578 reduced representation bisulfite sequencing protocols (318,929 CpGs); (iii) 6.5 Mb centered
579 around the *NR3C1* glucocorticoid receptor gene; and (iv) 100,099 loci included as a control for
580 genomic background that were randomly distributed across the hg38 human genome, excluding
581 centromeres, gaps, and Ns. Although the Y chromosome was included during the design of
582 control loci, we excluded the Y chromosome in analyses, resulting in 99,999 control loci which
583 fell into 98,967 unique 600 bp windows. Of these 98,967 windows, 94,679 contained CpG sites
584 and 4,288 did not, reflecting the sequence composition of the human genome as a whole. We
585 note that a single 600 bp genomic window could simultaneously include EPIC CpGs, *Msp1* CpG
586 cut sites, the *NR3C1* region, or control sites (i.e., assignment of windows to these compartments
587 are not mutually exclusive; Figure 1-figure supplement 1).
588 We then captured target regions from the sheared GM12878 DNA using SeqCap EZ
589 Prime Choice Probes (Roche), following the SeqCap EZ HyperCap protocol version 2.3. We
590 performed two capture reactions. We used 6 cycles for the Pre-Capture LM-PCR program and 16
591 cycles for the Post-Capture LM-PCR program. For the Post-Capture LM-PCR reaction, we used
592 the mSTARR_primerF2 and mstarr_primerR2 primers from Lea *et al.* (2018) to prepare the
593 DNA for ligation into the mSTARR plasmid. The resulting captured DNA was used as input for
594 the mSTARR-seq protocol (Lea *et al.*, 2018), beginning at the mSTARR-seq published protocol
595 step "Generate linearized mSTARR backbone for large-scale cloning".
596 We performed 4 and 6 replicate Gibson assemblies and transformations for the first and
597 second capture reactions, respectively. We then sequenced each transformation replicate on a
598 MiSeq to measure library diversity per replicate, with the following modifications to the
599 published mSTARR-seq protocol: we used 25 ul Kapa HiFi HotStart ReadyMix instead of 25 ul
600 NEB Q5 Hot start master mix, with the following cycle program: 98 C for 45 sec, 12 cycles of
601 98 C for 15 seconds, 60 C for 30 seconds, and 72 C for 60 seconds, followed by a final extension
602 at 72 C for 5 minutes. We measured library diversity of each transformation using the ENCODE
603 Project's PCR bottleneck coefficient (PBC), which is the percentage of non-duplicate mapped

604 reads from the total number of mapped reads (Landt *et al.*, 2012) (Supplementary File 21). We
605 pooled the ten transformations by weighting their molarities according to the PBCs to create the
606 final library. We then performed 8 re-transformations to expand the pooled library.
607 Replicate methyltransferase reactions and parallel mock methyltransferase reactions, in
608 which the *M. SssI* enzyme was replaced with water, were performed in 500 ul reactions, cleaned
609 with Ampure beads, and then pooled. The methylated DNA library and unmethylated DNA
610 library were each transfected into 18 replicate T75 flasks, each containing 12 million K562s,
611 with Lipofectamine 3000 (ThermoFisher Scientific) following the manufacturer's instructions.
612 42 hours post-transfection, replicates were treated with 2,000 U/mL IFNA2b (Thermo Fisher
613 Scientific), 1 uM dex (Sigma-Aldrich), or vehicle control (media). 48 hours post-transfection (6
614 hours post-treatment), cells were harvested for mSTARR-seq sequencing library generation. At
615 harvest, 5 x 10^5 cells were aliquoted separately into Buffer RLT to measure endogenous RNA
616 response to treatment, and 2 million cells were aliquoted for plasmid DNA extraction to measure
617 input DNA in each replicate. mSTARR RNA-seq and DNA-seq libraries were generated
618 following Lea *et al.* (2018). To measure endogenous gene expression from K562s in each
619 condition, we extracted RNA from the separately aliquoted cells using the Qiagen RNEasy kit
620 and prepared RNA-seq libraries using the NEBNext Ultra II RNA Library Prep Kit for Illumina.
621
622 *Comparison of mSTARR MD regulatory activity across cell types and experiments*
623 To assess cell type-specificity of methylation-dependent regulatory activity, we
624 transfected the mSTARR-seq library from Lea *et al.* (2018), comprised of 1:3 sheared genomic
625 DNA:*MspI*-digested DNA, into the HepG2 cell line. For the HepG2 experiment, we performed
626 one methyltransferase reaction and one sham methyltransferase reaction. Transfections were
627 performed with Lipofectamine 3000 (ThermoFisher Scientific) following the manufacturer's
628 instructions, with reagent quantities scaled to the following per replicate: 6.9 million HepG2
629 cells, 46 ug of DNA, 138 ul of Lipofectamine 3000, and 180 ul of P3000 (transfection enhancer
630 reagent). We performed all regulatory and MD regulatory analyses of HepG2 cells, as well as
631 analyses of K562s from a previously published smaller mSTARR-seq experiment (Lea *et al.*,
632 2018), following the same bioinformatics pipeline used for our main K562 experiment, described
633 below. To compare against previously published STARR-seq data in A549 cells, we identified
634 the union set of all regulatory peaks identified across six replicate STARR-seq experiments
635 collected at time point 0 in Johnson *et al.* (2018). To test for significant overlap between the
636 current K562 results and the other three data sets, we used Fisher's exact tests against a
637 background set of windows tested in both the current K562 experiment and each of the other data
638 sets.
639
640 *mSTARR-seq regulatory and MD regulatory analyses*
641 mSTARR RNA-seq and DNA-seq libraries were sequenced on the Illumina NovaSeq
642 platform as 100 basepair, paired-end reads (Supplementary File 1). Reads were trimmed with
643 Trim Galore (version 0.6.4) (Krueger, 2015) to remove basepairs at the ends of reads with Phred
644 scores less than 20 and stretches of 2 or more basepairs that matched adapter sequences.
645 Trimmed reads with a minimum length of 25 basepairs were retained. We mapped reads using
646 *bwa* (version 0.7.12) (Li and Durbin, 2009) using default settings. We retained read pairs that
647 mapped to a single best location using the *samtools* (version 1.3.1) (Li *et al.*, 2009) package
648 'view' command with options -q 10 -f 0x2. We segmented the genome into 600 bp, non-
649 overlapping windows, and used the bedtools (version 2.25.0) (Quinlan and Hall, 2010) *coverage*

function to count the number of RNA and DNA fragments overlapping each 600 bp window. We chose 600 bp for the genomic window size to accommodate our library's DNA fragment size (600-700 bp; Supplementary File 1), and because using smaller windows resulted in the identification of many adjacent windows as separate regulatory elements when they likely represent a single true enhancer (the median length of ENCODE-annotated enhancers is 600 bp).

For each of the 3 treatment conditions (baseline, IFNA, and dex), we reduced our dataset to windows for which at least three DNA samples in the methylated condition and three DNA samples in the unmethylated condition (i.e., 6 DNA samples total), and three RNA samples in *either* the methylated or unmethylated condition, had nonzero counts. One mSTARR RNA-seq sample in the baseline condition (sample ID L31250) was removed from further analysis because it had an unusually high proportion of zero counts in the testable windows; the corresponding paired DNA sample was therefore also removed prior to analysis (Supplementary File 1). Next, we retained only windows that showed high repeatability across DNA samples, following Lea *et al.* (2018). In brief, for each window we calculated the pairwise difference of read abundance for every pair of samples and created a distribution of all pairwise differences; windows were removed if at least 25% of pairs fell outside the central 90th percentile of the distribution (37,410 windows, 14.8% of the overall data set). On this reduced data set of testable windows, we performed voom normalization using the limma (version 3.44.3) *voomWithQualityWeights* function (Smyth, 2005; Law *et al.*, 2014), with methylation status included as a covariate in the design. We then used the *limma* function *lmFit* to apply the following model for each window:

$$y_i = \mu + m_i\beta_1 + s_i\beta_2 * I(m = 0) + s_i\beta_3 * I(m = 1) + \varepsilon_i$$

where y_i is the vector of normalized counts for n = 24 samples (12 RNA and 12 DNA samples; 22 samples for the baseline condition); μ is the intercept; m_i is methylation condition (0 = unmethylated; 1 = methylated) and β_1 its effect size; and I is an indicator variable in which β_2 and β_3 are the effects of sample type (s_i; 0 = DNA; 1 = RNA) in the unmethylated (m = 0) and methylated conditions (m =1), respectively. ε_i is the residual error.

To estimate the false discovery rate for identifying windows with regulatory activity (in either the methylated or unmethylated condition, or both), we compared the observed results to empirical null distributions generated using 100 permutations of RNA/DNA labels within each pair of samples following Storey and Tibshirani (2003). Unlike in the real data, in which most windows show a strong bias towards more reads in the DNA condition (because most windows exhibit no regulatory activity, and therefore show many more input DNA reads than RNA reads), permuted data results in relatively balanced effect sizes. Using the overall distribution of p-values to construct the null therefore substantially inflates the number of significant windows, but specifically because most observed windows have systematically *less* activity in the RNA condition than the DNA condition, not more (the direction of interest). Thus, retaining all p-values to construct the null leads to highly miscalibrated false discovery rates because the distribution of observed values is skewed towards smaller values—because of windows with "significantly" no regulatory activity—compared to the permuted data. To address this problem, for each permutation, we subsampled N windows with a positive sample type beta (corresponding to larger read counts in RNA samples versus DNA samples) in either the methylated condition, unmethylated condition, or both. Here, N is the number of windows with a positive sample type beta in the observed data (e.g., N = 17,461 in the baseline dataset). The p-

values from these windows were used to generate the empirical null. To define putative enhancer elements, we used an FDR cutoff of 1%.

To identify methylation-dependent enhancer activity, we focused on the windows that exhibited a positive sample type beta (i.e., exhibited more RNA reads than DNA reads) in either the methylated or unmethylated condition (or both) and tested for significant differences between β_2 and β_3 in the equation above (i.e., an interaction effect between RNA/DNA condition and the methylated/unmethylated condition). To estimate the false discovery rate for identifying methylation-dependent windows, we re-ran our main nested model on the same 100 sets of N windows each, in this case permuting methylation condition (unmethylated versus methylated) across sample pairs to generate the empirical null for the interaction effect of sample type (RNA versus DNA) * methylation condition (methylated or unmethylated). To define methylation-dependent regulatory elements, we again used an FDR cutoff of 1%.

To assess whether mSTARR RNA-seq and DNA-seq libraries were sequenced deeply enough to saturate detection of unique 600 bp windows included in the formal analyses, we used seqtk (https://github.com/lh3/seqtk) to randomly subset sequence reads from the raw fastq files for all RNA-seq or all DNA-seq replicates in the baseline dataset. We then applied to these data subsets the same filtering pipeline described above to generate a reduced data set of testable windows. The results of this rarefaction analysis (shown in Figure 1-figure supplement 4) shows that our sequencing depth is sufficient to capture all analyzable windows based on both the DNA read filter and the RNA read filter.

Enrichment of transcription factor binding motifs

To identify enrichment of potential transcription factor binding sites in the methylated condition, we used HOMER and motifs defined in the HOMER database (Heinz *et al.*, 2010) and the baseline treatment dataset to compare motifs within regulatory regions in the methylated condition, relative to motifs across all regulatory regions.

To identify potential transcription factor binding sites in windows with condition-specific regulatory or methylation-dependent regulatory activity, we first identified regions showing regulatory activity uniquely in the dex or IFNA conditions relative to both other conditions (based on an FDR of 1% to define regulatory activity). We used HOMER and motifs defined in the HOMER database to test for enrichment of transcription factor binding motifs within windows showing condition-specific regulatory activity relative to all windows tested for regulatory activity in that condition. We set a threshold of Bonferroni-corrected p-value < 0.01 to identify significantly enriched binding motifs.

Endogenous gene expression response of K562s to dex and IFNA

Endogenous RNA-seq libraries from K562 cells challenged with dex or IFNA were sequenced on an Illumina NovaSeq 6000 S1 flow cell as 100 base pair, paired-end reads. Reads were trimmed with Trim Galore (Trim Galore version 0.6.4_dev; Cutadapt version 2.3) to remove basepairs with a Phred score less than 20, and end sequences that matched at least two basepairs of the adapter sequence. Only trimmed reads longer than 25 basepairs were retained. We used the STAR package (version 2.5.0) (Dobin *et al.*, 2013) two-pass mapping to map the filtered reads to the hg38 genome. We retained uniquely mapped reads by filtering the output SAM file to keep reads with MAPQ = 255. We then used *htseq* (version 0.6.0) (Anders *et al.*, 2014) to quantify read counts per gene. We only retained genes that had TPM > 3 in at least 3 of

740 6 samples in at least one of the three conditions (baseline, IFNA, or dex). Only protein-coding
741 genes were retained for final analysis, resulting in a total of 10,676 testable genes.
742 We performed differential expression analysis separately for IFNA and dex, by subsetting
743 the data to the IFNA and baseline samples, or subsetting the data to the dex and baseline
744 samples. For each subset, we *voom* normalized the data (Law *et al.*, 2014), and used the *limma*
745 (Smyth, 2005) function *lmFit* to model the normalized gene expression as a function of
746 treatment, controlling for the percent of reads mapping to annotated features (to account for
747 technical variation in the efficiency of RNA purification during library prep) and methylation
748 condition for the associated sample. We calculated the FDR using the q-value approach of
749 (Storey and Tibshirani, 2003), based on an empirical null distribution that was derived from 100
750 permutations of treatment condition in the model.
751 To test whether genes were more responsive to IFNA stimulation if they were predicted
752 targets of IFNA-specific ISRE enhancers, we first used the bedtools *intersect* function to identify
753 the union set of ChIP-seq peaks for STAT1 and STAT2 (two of the three components of the
754 ISGF3 transcription factor that binds ISRE motifs; ENCODE accession numbers
755 ENCFF478XGE and ENCFF394KTR; ChIP-Seq data were not available for the third ISGF3
756 component, IRF9). We then reduced these regions to those showing significant, IFNA condition-
757 specific regulatory activity in the mSTARR-seq dataset (FDR < 1%). We used K562 enhancer-
758 gene links from EnhancerAtlas 2.0 (Gao *et al.*, 2016) to link the resulting IFNA-specific ISRE
759 enhancers to their target genes. Finally, we performed a two-sided, unpaired t-test to compare the
760 endogenous expression responses to IFNA for genes associated with putative IFNA-specific
761 ISRE enhancers relative to genes that are not associated with IFNA-specific ISRE enhancers.
762
763 *Endogenous gene expression and methylation in human macrophages*
764 To assess effects of DNA methylation-environment interactions on gene expression *in*
765 *vivo*, we evaluated endogenous methylation and gene expression from matched whole genome
766 bisulfite sequencing (WGBS) and RNA-seq data collected from human monocyte-derived
767 macrophages (n = 35 donors), with and without infection with the influenza A virus (IAV;
768 Aracena *et al.*, in press). Unsmoothed methylation counts were obtained for 19,492,906 loci in
769 both non-infected and IAV-infected samples (total n = 70) as described (Aracena *et al.*, in press).
770 We filtered loci to require coverage of ≥ 4 sequence reads in at least half of the non-infected or
771 IAV-infected samples. In the RNA-seq dataset for the same 35 individuals, we excluded any
772 genes that did not have an average RPKM > 2 in non-infected or IAV-infected samples. This
773 resulted in a total of 19,041,420 CpG sites and 14,122 genes used in downstream analyses.
774 We calculated normalization factors using calcNormFactors in edgeR (v 3.28.1)
775 (Robinson *et al.*, 2010) to scale the raw library sizes. We then used the voom function in limma
776 (v 3.42.2) (Smyth, 2005; Ritchie *et al.*, 2015) to apply the normalization factors, estimate the
777 mean-variance relationship, and convert raw read counts to log(CPM) values. Sequencing
778 batches were regressed out using ComBat from the sva Bioconductor package (v 3.34.0) (Leek *et*
779 *al.*, 2012), which fit a model that also included age (mean-centered) and admixture estimates. We
780 subsequently regressed out age effects using limma. Individual-wise fold-change (FC) matrices
781 were built by subtracting non-infected counts from IAV-infected counts for each individual using
782 weights calculated as in (Harrison *et al.*, 2019; Aracena *et al.*, in press).
783 For comparison of the mSTARR-seq dataset to the dataset from Aracena *et al.* (in press),
784 GrCh38/hg38 coordinates were lifted over to GRCh37/hg19 using the UCSC liftOver tool. We
785 required a 0.95 minimum ratio of bases that remap, excluded loci that output multiple regions,

786 set the minimum hit size in query to 0, and set the minimum chain size in the target to 0. The
787 GRCh37/hg19 coordinates were used in the following analyses.
788 We first sought to assess, within each of the 35 individuals, the correlation between
789 mSTARR-seq enhancer methylation levels at baseline (i.e., in non-infected cells) and
790 transcriptional responses of their nearest genes to IAV. To find overlaps between enhancer
791 regions and CpG loci, we used the *bedtools* intersect function (v2.29.1) with the "left outer join"
792 option. For each 600 bp mSTARR-seq enhancer region in each individual, we calculated the
793 mean methylation level across all overlapping CpGs. Each enhancer was linked to its nearest
794 gene, with a maximum distance of 100 kb, as described above. If an enhancer had multiple
795 linked genes (e.g., an enhancer that overlapped more than one gene), we took the mean
796 transcriptional response of all linked genes. For each individual, we calculated the Pearson's
797 correlation coefficient (r) between the DNA methylation levels within the mSTARR-seq-defined
798 enhancer windows, in non-infected cells, and transcriptional responses of their linked genes to
799 IAV infection. We also investigated the correlation between mean mSTARR-seq enhancer
800 window methylation and gene expression *within* non-infected and flu-infected samples
801 separately.
802 Finally, for each mSTARR-seq enhancer-gene pair, we sought to test the extent to which
803 average methylation level in the enhancer in non-infected samples explained the gene's
804 transcriptional response to IAV, across individuals. Here, we calculated the average CpG
805 methylation level for each 600 bp enhancer, after excluding CpGs with methylation variance less
806 than 0.01 across individuals. Thus, enhancers that did not contain any CpGs with appreciable
807 interindividual variation in DNA methylation levels were excluded from the analysis. This
808 filtering step resulted in 1,382 enhancer-gene pairs for this analysis. For each enhancer-gene pair,
809 we calculated the Pearson's correlation coefficient (and R^2) between the average methylation
810 level of the enhancer and the transcriptional response of the linked gene. P-values were corrected
811 for multiple hypothesis testing using the q-value method in R (Storey and Tibshirani, 2003).
812
813 *CpG methylation associated with early life adversity*
814 We performed a literature search to identify studies for which CpG methylation
815 differences have been linked to adverse conditions during early life. We considered all journal
816 articles that contained the words "early life adversity" and "Infinium" on
817 https://scholar.google.com on May 10, 2021, which produced 269 results. We required that the
818 study evaluated CpG methylation using an Illumina Infinium array (27K, 450K, or EPIC), and
819 that the article provided Infinium CpG probe IDs or CpG genomic coordinates of candidate
820 CpGs. Articles that reported no significant CpG sites, but still reported "top" CpG sites, were
821 retained. Articles that performed analyses to identify differentially methylated regions (DMRs;
822 as opposed to CpG site-by-site analysis), and then reported individual CpG sites within the
823 candidate DMRs, were retained. We considered early life adversity to encompass both social and
824 nonsocial sources of environmental adversity (e.g., exposure to severe weather), any time from
825 prenatal development to 18 years of age. We did not impose criteria for cell type or subject age
826 at time of sampling. See Figure 4-figure supplement 1 and Supplementary File 20 for a summary
827 of the resulting studies.
828 For each study dataset, we performed a Fisher's exact test to test whether ELA candidate
829 sites, relative to the total set of CpG sites on the Illumina array used in that study (450K, EPIC,
830 or 27K array), were enriched in the mSTARR-seq regulatory windows we identified in the
831 baseline, dex, or IFNA condition.

Acknowledgments
We thank B.J. Nielsen, Tawni Voyles, and Tina Del Carpio for their contributions to data generation, Terrie Moffitt and the Reddy lab at Duke University for project feedback, Graham Johnson for sharing the A549 data, Courtney Karner for use of equipment, Xiang Zhou for constructive advice on statistical modeling, and two anonymous reviewers for constructive feedback on an earlier version of this manuscript. This study was supported by the National Institutes of Health (R01HD088558 to J.T. and F32HD095616 to R.A.J.), the Canadian Institutes for Advanced Research Child Brain and Development Program, a Sloan Foundation Early Career Research Fellowship to J.T., and a Foerster-Bernstein Postdoctoral Fellowship to R.A.J. High-performance computing resources were supported by the North Carolina Biotechnology Center (Grant Number 2016-IDG-1013 and 2020-IIG-2109).

Data Availability
mSTARR-seq RNA and DNA sequencing data generated in this study for K562 and HepG2 cells are available in the NCBI Sequence Read Archive (SRA; BioProject accession number PRJNA922490). K562 endogenous RNA-seq data are available in the NCBI Gene Expression Omnibus (GEO series accession GSE222643). The previously published data from (Lea *et al.*, 2018) used in this study are available in NCBI's SRA accession number SRP120556. The previously published A549 data from (Johnson *et al.*, 2018) were kindly provided by Graham Johnson. The sequencing data for the macrophage RNA-seq and WGBS datasets are available at the European Genome-Phenome Archive (EGA) under accession numbers EGAD00001008422 and EGAD00001008359, respectively. The zenodo repository at https://zenodo.org/record/7949036#.ZGZ5UnbMJq9 provides the code used for analyses, as well as track files (compatible with the UCSC genome browser) for mSTARR-seq hg38 windows with regulatory activity, and windows with methylation-dependent regulatory activity, in all three conditions (baseline, IFNA, and dex). The mSTARR-seq plasmid, *pmSTARRseq1* is available through AddGene.

Figure Supplements
Figure 1-figure supplement 1. Overlap of target genomic regions with each other.

Figure 1-figure supplement 2. mSTARR-seq library diversity.

Figure 1-figure supplement 3. Methylation levels of mSTARR-seq DNA, pre- and post-transfection.

Figure 1-figure supplement 4. Rarefaction curve showing total number of windows formally tested for regulatory activity, as a function of number of reads sequenced per DNA or RNA replicate.

Figure 1-figure supplement 5. Overlap of regulatory activity across datasets.

Figure 1-figure supplement 6. Correlations between RNA and DNA replicates.

Figure 1-figure supplement 7. Library diversity and regions of regulatory activity in HepG2

878 cells.
879
880 Figure 1-figure supplement 8. Methylation-dependent regulatory activity across datasets.
881
882 Figure 1-figure supplement 9. RNA to DNA ratios in the methylated and unmethylated replicates
883 in the baseline dataset.
884
885 Figure 1-figure supplement 10. Histograms of RNA to DNA ratios in the baseline dataset.
886
887 Figure 1-figure supplement 11. Relationship between CpG density and methylation-dependent
888 regulatory activity.
889
890 Figure 2-figure supplement 1. Filtering results across datasets.
891
892 Figure 2-figure supplement 2. Overlap of tested genomic windows across datasets.
893
894 Figure 2-figure supplement 3. Overlap of regulatory activity and effects of methylation across
895 environmental conditions.
896
897 Figure 2-figure supplement 4. *IFIT5* endogenous gene expression is responsive to IFNA
898 stimulation.
899
900 Figure 3-figure supplement 1. Across individuals, methylation in the mSTARR-seq annotated
901 enhancer chr1:1013400-1014000 predicts the *ISG15* gene expression response to flu.
902
903 Figure 4-figure supplement 1. Summary of early-life adversity (ELA) studies.
904
905 **Supplementary Files**
906 Supplementary File 1. Table summarizing the K562 mSTARR-seq DNA and RNA libraries
907 generated in this study.
908
909 Supplementary File 2. Table providing sequencing depth and CpG composition statistics for the
910 target regions (EPIC array, RRBS, *NR3C1*, and control) in the baseline dataset.
911
912 Supplementary File 3. Table of results from the model testing for methylation-dependent
913 regulatory activity in K562 cells at baseline.
914
915 Supplementary File 4. Table of enrichment results of mSTARR-seq regulatory regions for
916 ENCODE-defined chromosome states.
917
918 Supplementary File 5. Table providing sequencing depth and CpG composition statistics for the
919 baseline dataset and Lea *et al*., 2018 dataset.
920
921 Supplementary File 6. Table of results from the model testing for methylation-dependent
922 regulatory activity in K562 cells at baseline condition using the dataset from (Lea *et al.*, 2018).
923

924 Supplementary File 7. Table of results from the model testing for methylation-dependent
925 regulatory activity in HepG2 cells at baseline.
926
927 Supplementary File 8. Table of enrichment results of transcription factor binding motifs for
928 regulatory windows with higher activity in the methylated relative to the sham condition.
929
930 Supplementary File 9. Table providing the number of 600 bp windows passing each filter for the
931 baseline, IFNA, dex, and HepG2 datasets.
932
933 Supplementary File 10. Table of results from the model testing for methylation-dependent
934 regulatory activity in K562 cells stimulated with IFNA.
935
936 Supplementary File 11. Table of results from the model testing for methylation-dependent
937 regulatory activity in K562 cells stimulated with dex.
938
939 Supplementary File 12. Table of enrichment results of transcription factor binding motifs for
940 regulatory windows specific to the IFNA treatment (<1% FDR in IFNA and >1% FDR in
941 baseline and Dex).
942
943 Supplementary File 13. Table of enrichment results of transcription factor binding motifs for
944 regulatory windows specific to the Dex treatment (<1% FDR in Dex and >1% FDR in baseline
945 and IFNA).
946
947 Supplementary File 14. Table of enrichment results of transcription factor binding motifs for
948 regulatory windows specific to the IFNA treatment (<1% FDR in IFNA and >10% FDR in
949 baseline and Dex).
950
951 Supplementary File 15. Table of enrichment results of transcription factor binding motifs for
952 regulatory windows specific to the Dex treatment (<1% FDR in Dex and >10% FDR in baseline
953 and IFNA).
954
955 Supplementary File 16. Table of results from the model testing for the K562 endogenous gene
956 expression response to IFNA.
957
958 Supplementary File 17. Table of Pearson's correlation results, within individuals, between
959 mSTARR-seq enhancer DNA methylation in non-infected macrophages and transcriptional
960 response of nearest genes upon IAV infection.
961
962 Supplementary File 18. Table of Pearson's correlation results, within individuals, between
963 mSTARR-seq enhancer DNA methylation in non-infected macrophages and gene expression
964 level in non-infected or IAV-infected macrophages.
965
966 Supplementary File 19. Table of Pearson's correlation results, across individuals, between
967 mSTARR-seq enhancer DNA methylation in non-infected macrophages and transcriptional
968 response of nearest genes upon IAV infection.
969

970 Supplementary File 20. Table of enrichment results of regulatory activity in early-life adversity
971 associated CpGs relative to regulatory activity in all CpGs on the associated Illumina array.
972
973 Supplementary File 21. Library diversity of replicate transformations using the ENCODE
974 Project's PCR bottleneck coefficient (PBC).

975 **References**

976 Anders S, Pyl PT, Huber W (2014) HTSeq–A Python framework to work with high-
977 throughput sequencing data. Bioinformatics, btu638.
978 Aracena KA, Lin YL, Luo K, Pacis A, Gona S, Mu Z, Yotova V, Sindeaux R, Pramatarova A,
979 Simon MM, Chen X, Groza C, Lougheed D, Gregoire R, Brownlee D, Boyce C, Pique-
980 Regi R, Li Y, He X, Bujold D, Pastinen T, Bourque G, Barreiro LB. Epigenetic variation
981 impacts individual differences in the transcriptional response to influenza infection.
982 Nature Genetics. **In press**.
983 Aristizabal MJ, Anreiter I, Halldorsdottir T, Odgers CL, McDade TW, Goldenberg A,
984 Mostafavi S, Kobor MS, Binder EB, Sokolowski MB (2020) Biological embedding of
985 experience: A primer on epigenetics. Proceedings of the National Academy of
986 Sciences, **117**, 23261-23269.
987 Arnold CD, Gerlach D, Stelzer C, Boryń ŁM, Rath M, Stark A (2013) Genome-wide
988 quantitative enhancer activity maps identified by STARR-seq. Science, **339**, 1074-
989 1077.
990 Cain DW, Cidlowski JA (2017) Immune regulation by glucocorticoids. Nature Reviews
991 Immunology, **17**, 233-247.
992 Cao-Lei L, Massart R, Suderman MJ, Machnes Z, Elgbeili G, Laplante DP, Szyf M, King S
993 (2014) DNA methylation signatures triggered by prenatal maternal stress exposure
994 to a natural disaster: Project Ice Storm. PloS one, **9**, e107653.
995 Chaudhri VK, Dienger-Stambaugh K, Wu Z, Shrestha M, Singh H (2020) Charting the cis-
996 regulome of activated B cells by coupling structural and functional genomics. Nature
997 Immunology, **21**, 210-220.
998 Chen K, Liu J, Cao X (2017) Regulation of type I interferon signaling in immunity and
999 inflammation: A comprehensive review. Journal of autoimmunity, **83**, 1-11.
1000 Demetriou CA, van Veldhoven K, Relton C, Stringhini S, Kyriacou K, Vineis P (2015)
1001 Biological embedding of early‐life exposures and disease risk in humans: a role for
1002 DNA methylation. European journal of clinical investigation, **45**, 303-332.
1003 Dobin A, Davis CA, Schlesinger F, Drenkow J, Zaleski C, Jha S, Batut P, Chaisson M, Gingeras
1004 TR (2013) STAR: ultrafast universal RNA-seq aligner. Bioinformatics, **29**, 15-21.
1005 Dolinoy DC, Weidman JR, Waterland RA, Jirtle RL (2006) Maternal genistein alters coat
1006 color and protects Avy mouse offspring from obesity by modifying the fetal
1007 epigenome. Environmental health perspectives, **114**, 567-572.
1008 Dubois M, Louvel S, Le Goff A, Guaspare C, Allard P (2019) Epigenetics in the public sphere:
1009 interdisciplinary perspectives. Environmental Epigenetics, **5**, dvz019.
1010 Eisenberger NI, Cole SW (2012) Social neuroscience and health: neurophysiological
1011 mechanisms linking social ties with physical health. Nature neuroscience, **15**, 669-
1012 674.
1013 ENCODE (2012) An integrated encyclopedia of DNA elements in the human genome.
1014 Nature, **489**, 57.
1015 Ernst J, Kellis M (2012) ChromHMM: automating chromatin-state discovery and
1016 characterization. Nature methods, **9**, 215-216.
1017 Fanucchi S, Domínguez-Andrés J, Joosten LA, Netea MG, Mhlanga MM (2021) The
1018 intersection of epigenetics and metabolism in trained immunity. Immunity, **54**, 32-
1019 43.

1020 Gallego Romero I, Lea AJ (2022) Leveraging massively parallel reporter assays for
1021 evolutionary questions. arXiv e-prints, arXiv: 2204.05857.
1022 Gao T, He B, Liu S, Zhu H, Tan K, Qian J (2016) EnhancerAtlas: a resource for enhancer
1023 annotation and analysis in 105 human cell/tissue types. Bioinformatics, **32**, 3543-
1024 3551.
1025 Greenberg MV, Bourc'his D (2019) The diverse roles of DNA methylation in mammalian
1026 development and disease. Nature reviews Molecular cell biology, **20**, 590-607.
1027 Harrison GF, Sanz J, Boulais J, Mina MJ, Grenier J-C, Leng Y, Dumaine A, Yotova V, Bergey
1028 CM, Nsobya SL (2019) Natural selection contributed to immunological differences
1029 between hunter-gatherers and agriculturalists. Nature ecology & evolution, **3**, 1253-
1030 1264.
1031 Heinz S, Benner C, Spann N, Bertolino E, Lin YC, Laslo P, Cheng JX, Murre C, Singh H, Glass
1032 CK (2010) Simple combinations of lineage-determining transcription factors prime
1033 cis-regulatory elements required for macrophage and B cell identities. Molecular
1034 cell, **38**, 576-589.
1035 Hertzman C (1999) The biological embedding of early experience and its effects on health
1036 in adulthood. Annals of the New York Academy of Sciences, **896**, 85-95.
1037 Hertzman C (2012) Putting the concept of biological embedding in historical perspective.
1038 Proceedings of the National Academy of Sciences, **109**, 17160-17167.
1039 Hertzman C, Boyce T (2010) How experience gets under the skin to create gradients in
1040 developmental health. Annual review of public health, **31**, 329-347.
1041 Husquin LT, Rotival M, Fagny M, Quach H, Zidane N, McEwen LM, MacIsaac JL, Kobor MS,
1042 Aschard H, Patin E (2018) Exploring the genetic basis of human population
1043 differences in DNA methylation and their causal impact on immune gene regulation.
1044 Genome biology, **19**, 1-17.
1045 Johnson GD, Barrera A, McDowell IC, D'Ippolito AM, Majoros WH, Vockley CM, Wang X,
1046 Allen AS, Reddy TE (2018) Human genome-wide measurement of drug-responsive
1047 regulatory activity. Nature communications, **9**, 1-9.
1048 Kamada R, Yang W, Zhang Y, Patel MC, Yang Y, Ouda R, Dey A, Wakabayashi Y, Sakaguchi K,
1049 Fujita T (2018) Interferon stimulation creates chromatin marks and establishes
1050 transcriptional memory. Proceedings of the National Academy of Sciences, **115**,
1051 E9162-E9171.
1052 Kazachenka A, Bertozzi TM, Sjoberg-Herrera MK, Walker N, Gardner J, Gunning R, Pahita E,
1053 Adams S, Adams D, Ferguson-Smith AC (2018) Identification, characterization, and
1054 heritability of murine metastable epialleles: implications for non-genetic
1055 inheritance. Cell, **175**, 1259-1271. e1213.
1056 Killip MJ, Fodor E, Randall RE (2015) Influenza virus activation of the interferon system.
1057 Virus research, **209**, 11-22.
1058 Klein JC, Agarwal V, Inoue F, Keith A, Martin B, Kircher M, Ahituv N, Shendure J (2020) A
1059 systematic evaluation of the design and context dependencies of massively parallel
1060 reporter assays. Nature Methods, **17**, 1083-1091.
1061 Koss KJ, Gunnar MR (2018) Annual research review: Early adversity, the hypothalamic–
1062 pituitary–adrenocortical axis, and child psychopathology. Journal of Child
1063 Psychology and Psychiatry, **59**, 327-346.

1064 Kreibich E, Kleinendorst R, Barzaghi G, Kaspar S, Krebs AR (2023) Single-molecule
1065 footprinting identifies context-dependent regulation of enhancers by DNA
1066 methylation. Molecular Cell.
1067 Kribelbauer JF, Laptenko O, Chen S, Martini GD, Freed-Pastor WA, Prives C, Mann RS,
1068 Bussemaker HJ (2017) Quantitative analysis of the DNA methylation sensitivity of
1069 transcription factor complexes. Cell reports, **19**, 2383-2395.
1070 Krueger F (2015) Trim Galore.
1071 http://wwwbioinformaticsbabrahamacuk/projects/trim_galore/.
1072 Landt SG, Marinov GK, Kundaje A, Kheradpour P, Pauli F, Batzoglou S, Bernstein BE, Bickel
1073 P, Brown JB, Cayting P (2012) ChIP-seq guidelines and practices of the ENCODE and
1074 modENCODE consortia. Genome research, **22**, 1813-1831.
1075 Law CW, Chen Y, Shi W, Smyth GK (2014) Voom: precision weights unlock linear model
1076 analysis tools for RNA-seq read counts. Genome biology, **15**, R29.
1077 Lea AJ, Vockley CM, Johnston RA, Del Carpio CA, Barreiro LB, Reddy TE, Tung J (2018)
1078 Genome-wide quantification of the effects of DNA methylation on human gene
1079 regulation. Elife, **7**, e37513.
1080 Leek JT, Johnson WE, Parker HS, Jaffe AE, Storey JD (2012) The sva package for removing
1081 batch effects and other unwanted variation in high-throughput experiments.
1082 Bioinformatics, **28**, 882-883.
1083 Lei Y, Zhang X, Su J, Jeong M, Gundry MC, Huang Y-H, Zhou Y, Li W, Goodell MA (2017)
1084 Targeted DNA methylation in vivo using an engineered dCas9-MQ1 fusion protein.
1085 Nature communications, **8**, 1-10.
1086 Li H, Durbin R (2009) Fast and accurate short read alignment with Burrows–Wheeler
1087 transform. Bioinformatics, **25**, 1754-1760.
1088 Li H, Handsaker B, Wysoker A, Fennell T, Ruan J, Homer N, Marth G, Abecasis G, Durbin R
1089 (2009) The sequence alignment/map format and SAMtools. Bioinformatics, **25**,
1090 2078-2079.
1091 Liu PZ, Nusslock R (2018) How stress gets under the skin: early life adversity and
1092 glucocorticoid receptor epigenetic regulation. Current genomics, **19**, 653-664.
1093 Maeder ML, Angstman JF, Richardson ME, Linder SJ, Cascio VM, Tsai SQ, Ho QH, Sander JD,
1094 Reyon D, Bernstein BE (2013) Targeted DNA demethylation and activation of
1095 endogenous genes using programmable TALE-TET1 fusion proteins. Nature
1096 biotechnology, **31**, 1137-1142.
1097 Meissner A, Gnirke A, Bell GW, Ramsahoye B, Lander ES, Jaenisch R (2005) Reduced
1098 representation bisulfite sequencing for comparative high-resolution DNA
1099 methylation analysis. Nucleic acids research, **33**, 5868-5877.
1100 O'Malley RC, Huang S-sC, Song L, Lewsey MG, Bartlett A, Nery JR, Galli M, Gallavotti A, Ecker
1101 JR (2016) Cistrome and epicistrome features shape the regulatory DNA landscape.
1102 Cell, **165**, 1280-1292.
1103 Ostuni R, Piccolo V, Barozzi I, Polletti S, Termanini A, Bonifacio S, Curina A, Prosperini E,
1104 Ghisletti S, Natoli G (2013) Latent enhancers activated by stimulation in
1105 differentiated cells. Cell, **152**, 157-171.
1106 Pacis A, Mailhot-Léonard F, Tailleux L, Randolph HE, Yotova V, Dumaine A, Grenier J-C,
1107 Barreiro LB (2019) Gene activation precedes DNA demethylation in response to
1108 infection in human dendritic cells. Proceedings of the National Academy of Sciences,
1109 **116**, 6938-6943.

1110 Pacis A, Tailleux L, Morin AM, Lambourne J, MacIsaac JL, Yotova V, Dumaine A, Danckaert A,
1111 Luca F, Grenier J-C (2015) Bacterial infection remodels the DNA methylation
1112 landscape of human dendritic cells. Genome research, **25**, 1801-1811.
1113 Perng Y-C, Lenschow DJ (2018) ISG15 in antiviral immunity and beyond. Nature Reviews
1114 Microbiology, **16**, 423-439.
1115 Provençal N, Arloth J, Cattaneo A, Anacker C, Cattane N, Wiechmann T, Röh S, Ködel M,
1116 Klengel T, Czamara D (2020) Glucocorticoid exposure during hippocampal
1117 neurogenesis primes future stress response by inducing changes in DNA
1118 methylation. Proceedings of the National Academy of Sciences, **117**, 23280-23285.
1119 Quinlan AR, Hall IM (2010) BEDTools: a flexible suite of utilities for comparing genomic
1120 features. Bioinformatics, **26**, 841-842.
1121 Ritchie ME, Phipson B, Wu D, Hu Y, Law CW, Shi W, Smyth GK (2015) limma powers
1122 differential expression analyses for RNA-sequencing and microarray studies.
1123 Nucleic acids research, **43**, e47-e47.
1124 Robinson MD, McCarthy DJ, Smyth GK (2010) edgeR: a Bioconductor package for
1125 differential expression analysis of digital gene expression data. bioinformatics, **26**,
1126 139-140.
1127 Sardina JL, Collombet S, Tian TV, Gómez A, Di Stefano B, Berenguer C, Brumbaugh J,
1128 Stadhouders R, Segura-Morales C, Gut M (2018) Transcription factors drive Tet2-
1129 mediated enhancer demethylation to reprogram cell fate. Cell stem cell, **23**, 727-
1130 741. e729.
1131 Shlyueva D, Stampfel G, Stark A (2014) Transcriptional enhancers: from properties to
1132 genome-wide predictions. Nature Reviews Genetics, **15**, 272-286.
1133 Smyth GK (2005) Limma: linear models for microarray data. In: Bioinformatics and
1134 computational biology solutions using R and Bioconductor, pp. 397-420. Springer.
1135 Storey JD, Tibshirani R (2003) Statistical significance for genomewide studies. Proc Natl
1136 Acad Sci U S A, **100**, 9440-9445.
1137 Sun S, Barreiro LB (2020) The epigenetically-encoded memory of the innate immune
1138 system. Current opinion in immunology, **65**, 7-13.
1139 Yim YY, Teague CD, Nestler EJ (2020) In vivo locus-specific editing of the neuroepigenome.
1140 Nature Reviews Neuroscience, **21**, 471-484.
1141 Yin Y, Morgunova E, Jolma A, Kaasinen E, Sahu B, Khund-Sayeed S, Das PK, Kivioja T, Dave
1142 K, Zhong F (2017) Impact of cytosine methylation on DNA binding specificities of
1143 human transcription factors. Science, **356**, eaaj2239.
1144
1145

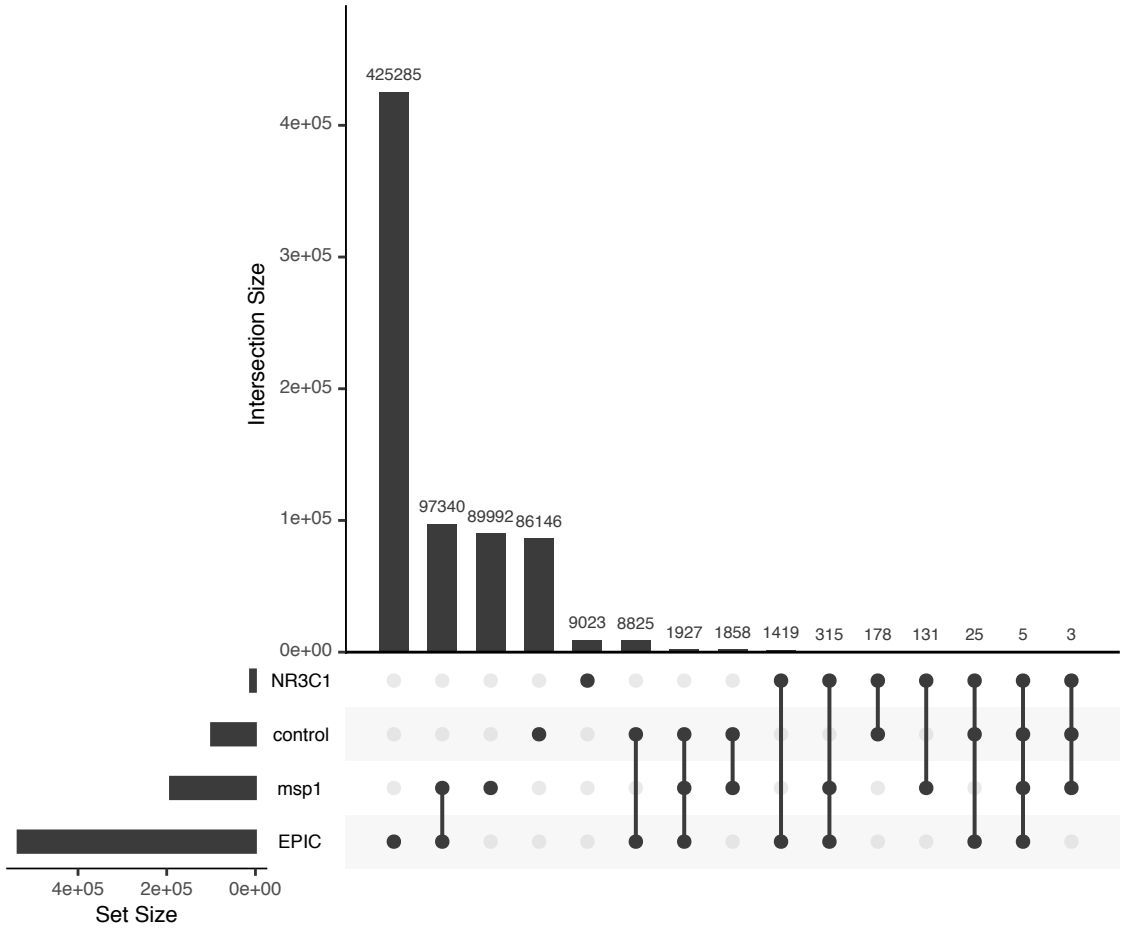

Figure 1-figure supplement 1. Overlap of target genomic regions with each other. Upset plot showing the degree to which 600 bp non-overlapping genomic windows are shared between the four target genomic regions (EPIC CpGs, *Msp1* CpG cut sites, the *NR3C1* region, or control sites). Overlap occurs because a single 600 bp genomic window can simultaneously include EPIC CpGs, *Msp1* CpG cut sites, the *NR3C1* region, and/or control sites. This plot includes 722,472 unique windows, reflecting the set of windows containing at least 1 basepair of sequence in the target loci.

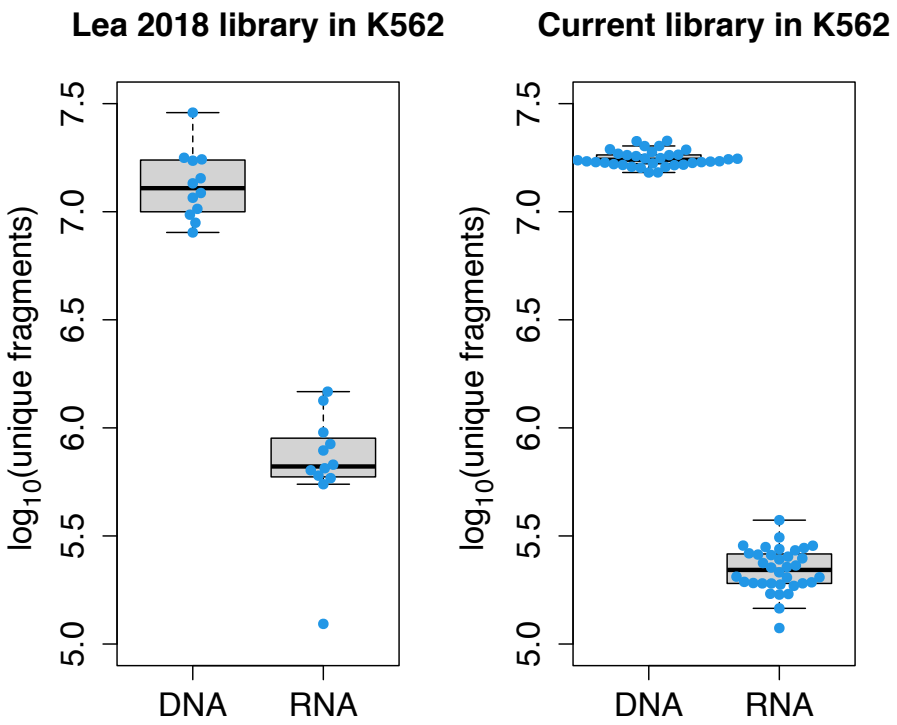

1153 **Figure 1-figure supplement 2. mSTARR-seq library diversity.** Comparison of diversity of
1154 unique mSTARR-seq DNA and RNA fragments from the library generated in this study
1155 (transfected into K562 cells) relative to the library published in Lea *et al*., 2018 (independently
1156 transfected into K562 cells). Each dot represents an experimental replicate. Each box represents
1157 the interquartile range, with the median value depicted as a horizontal bar. Whiskers extend to
1158 the most extreme values within 1.5x of the interquartile range.

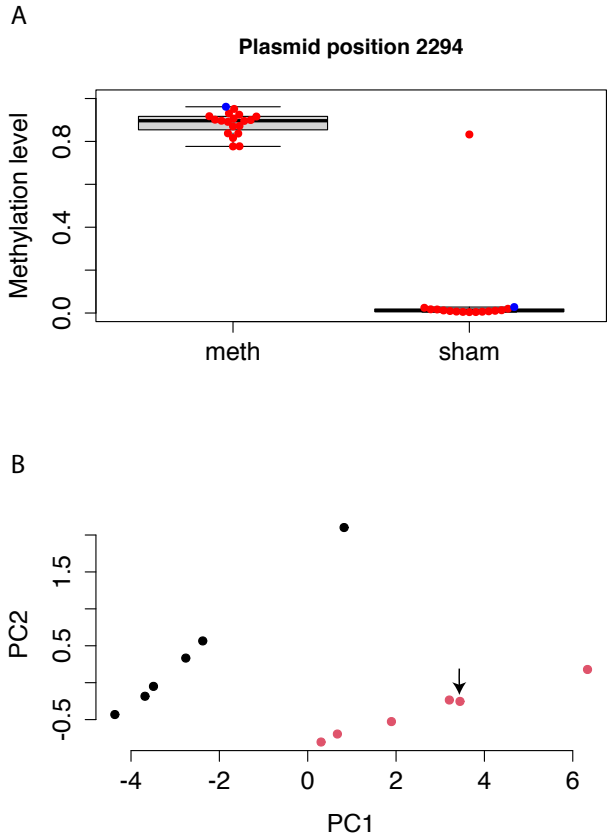

Figure 1-figure supplement 3. Methylation levels of mSTARR-seq DNA, pre- and post-transfection. (A) Bisulfite sequencing shows that DNA methylation on the mSTARR-seq plasmid is maintained until the end of the experiment (i.e., 48 hours after transfection), with significantly higher methylation levels in the replicates from the methyltransferase reaction relative to the replicates from the sham methyltransferase reaction (mean methylated = 0.885, mean unmethylated = 0.066; unpaired t-test: t = -14.66, df = 15,124, p = 2.39 x 10^{-10}). Each dot represents an experimental replicate. Red dots indicate post-transfection DNA samples; the single blue dot per condition indicates pre-transfection DNA methylation levels. Methylation estimates are based on the CpG at the position 2294, which is located in the plasmid region used for Gibson assembly. We assessed methylation of this CpG, rather than across CpGs genome-wide, because the genomic coverage of our bisulfite sequencing data across replicates was too variable to perform reliable site-by-site analysis of DNA methylation levels before and after the 48 hour experiment. One sample from the dex sham reaction, L31395, shows an unexpectedly high level of methylation, which appears to be due to an error during generation of the bisulfite sequencing library (e.g., mislabeled tube or poor bisulfite conversion), and not the experimental replicate of cells itself, as the mSTARR-seq RNA library (L31244) from the same replicate clusters with the unmethylated sham replicates as expected (panel B). **(B)** The first two principal components summarizing overall counts of mSTARR-seq reads for the dex-treated RNA samples (i.e., the raw readout of overall regulatory activity). Each dot represents an experimental replicate, with red and black indicating sham and methylated replicates, respectively. Overall regulatory activity of sample L31244 (indicated by arrow) clusters with the sham replicates as expected, suggesting that this replicate was indeed transfected with sham-treated mSTARR-seq DNA.

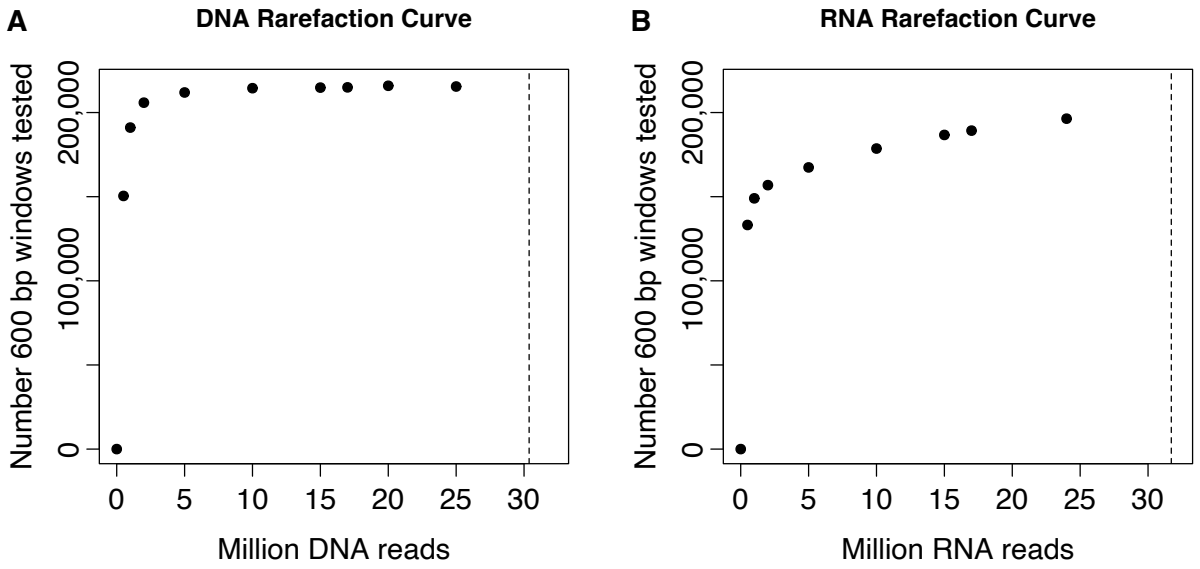

Figure 1-figure supplement 4. Rarefaction curve showing total number of windows formally tested for regulatory activity, as a function of number of reads sequenced per DNA or RNA replicate. Sequencing reads from the (A) DNA replicates or (B) RNA replicates of the baseline dataset were rarefied to the values shown on the x-axis before running the data processing steps and applying the filtering criteria described in the Materials and Methods for the full data set. Dashed vertical lines represent the mean number of sequenced reads per DNA replicate (mean [SD] = 30.375 million [3.335 million]) or RNA replicate (mean [SD] = 31.712 million [8.194 million]) in the full baseline dataset. These analyses show that our sequencing effort saturated the number of formally analyzable windows based on either our criteria for inclusion based on DNA library sequencing depth or RNA library sequencing depth.

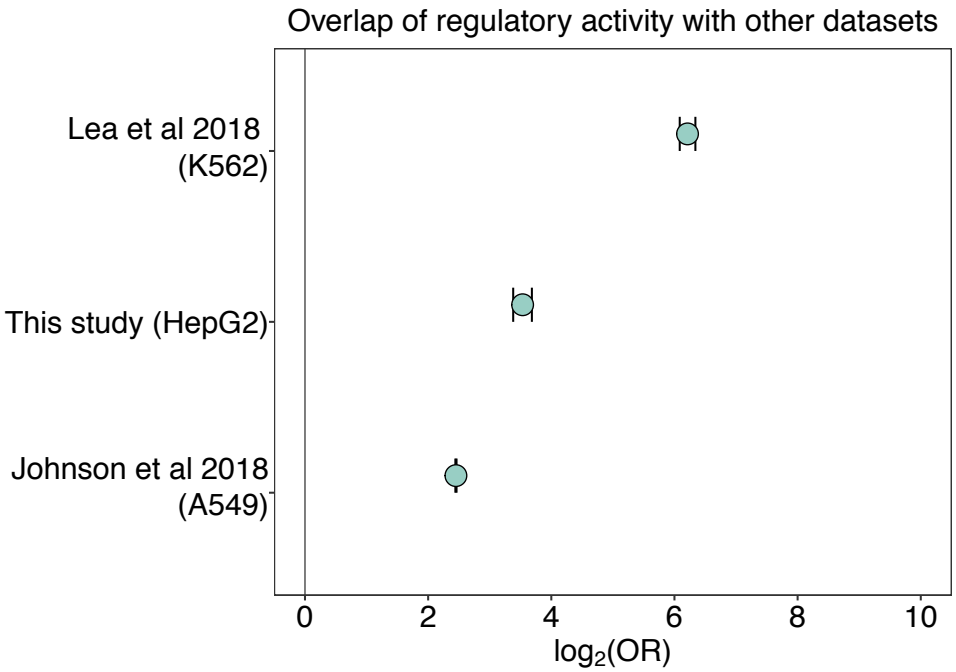

Figure 1-figure supplement 5. Overlap of regulatory activity across datasets. Regulatory regions (in either the unmethylated sham condition, the methylated condition, or both) identified via mSTARR-seq in this study significantly overlap with: K562 regulatory regions (in either the unmethylated sham or methylated condition, or both) from a previously generated mSTARR-seq dataset reanalyzed with our pipeline (Lea et al., 2018) ($\log_2$(OR) [95% CI] = 6.212 [6.086, 6.440], $p < 1.0 \times 10^{-300}$); regulatory regions (in either the unmethylated sham or methylated condition, or both) from an mSTARR-seq experiment in HepG2 liver cells ($\log_2$(OR) [95% CI] = 3.534 [3.381, 3.684], $p = 5.21 \times 10^{-307}$); and regulatory regions from a conventional STARR-seq experiment (i.e., an unmethylated condition) in A549 lung epithelial cells (Johnson et al., 2018) ($\log_2$(OR) [95% CI] = 2.451 [2.442, 2.461], $p < 1.0 \times 10^{-300}$). Bars represent 95% confidence intervals.

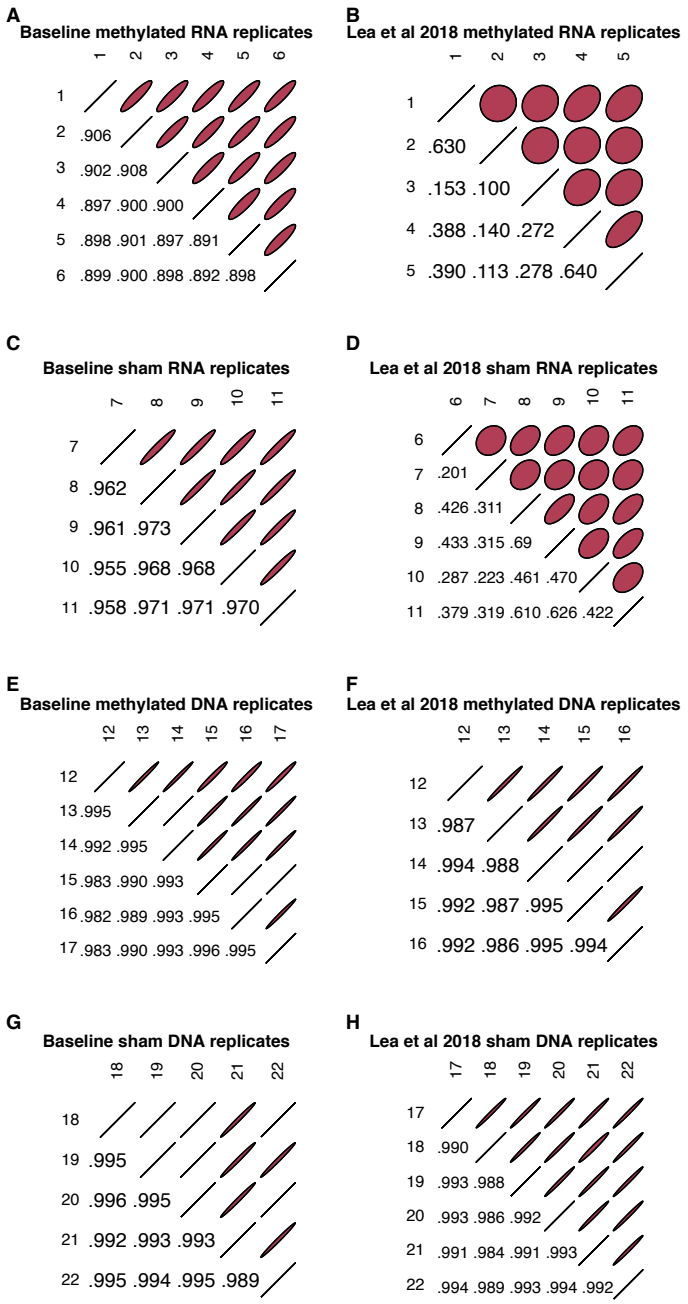

Figure 1-figure supplement 6. Correlations between RNA and DNA replicates. Pearson correlations (r) of raw counts between RNA replicates (A-D) and between DNA replicates (E-H) within the windows we formally analyzed for enhancer activity in the baseline dataset reported here and in Lea *et al*., 2018, following a uniform data processing pipeline. All replicate pairs (both RNA and DNA, in both sham and methylated conditions) in the baseline dataset show correlations ≥ 0.89, demonstrating replicate reproducibility comparable to other STARR-seq studies (e.g., Klein et al., 2020). For RNA libraries, replicates in the baseline dataset are more correlated than in the Lea *et al*., 2018 dataset (RNA replicates: baseline mean r = 0.926; Lea *et al*., 2018 mean r = 0.347), although DNA replicates show similar inter-replicate consistency (baseline mean r = 0.992; *Lea et al*., 2018 mean r = 0.991).

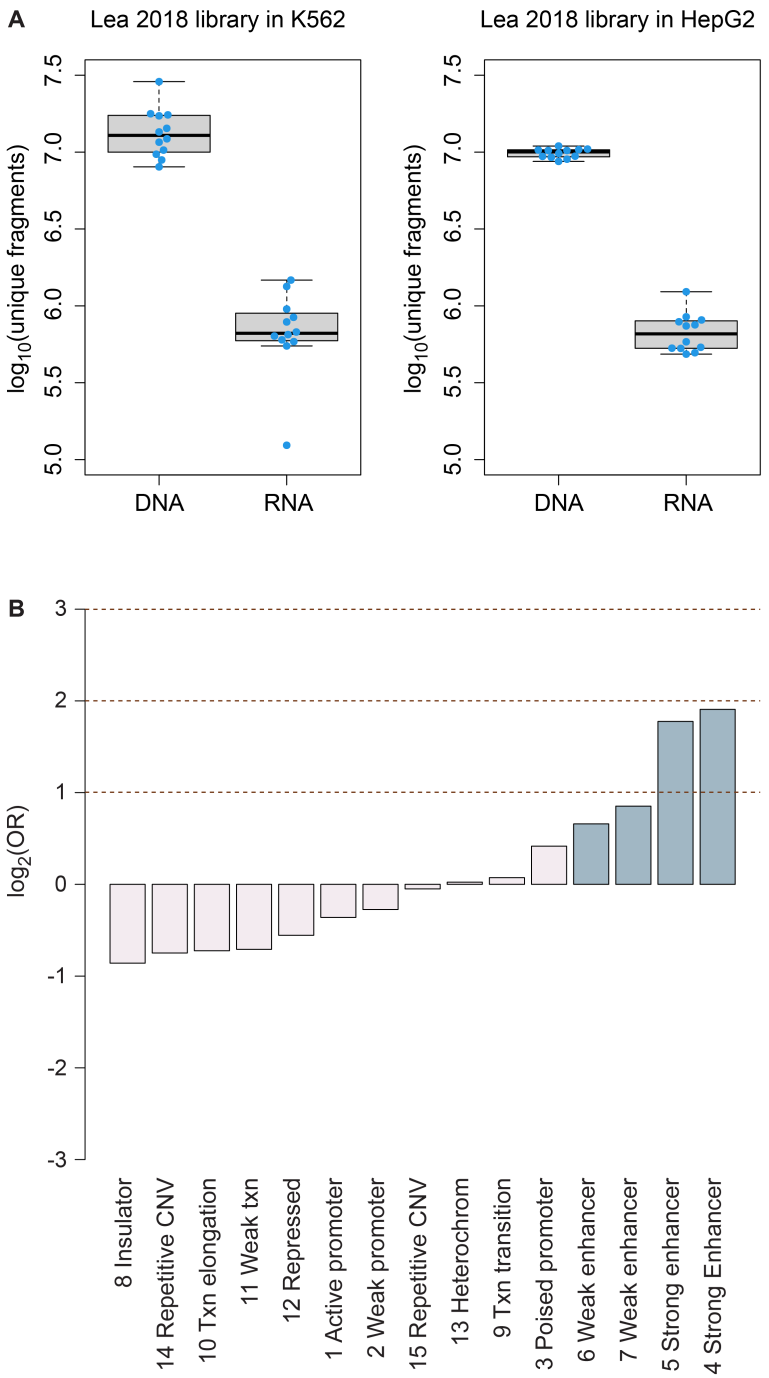

Figure 1-figure supplement 7. Library diversity and regions of regulatory activity in HepG2 cells. (A) Comparison of diversity of unique mSTARR-seq DNA and RNA fragments from the library published in Lea *et al*., 2018 (transfected into K562 cells) versus the same library transfected into HepG2 cells in this study. Each dot represents an experimental replicate. Each box represents the interquartile range, with the median value depicted as a horizontal bar. Whiskers extend to the most extreme values within 1.5x of the interquartile range. **(B)** mSTARR-seq regulatory activity in HepG2 cells is strongly enriched in ENCODE-defined enhancers (indicated in blue) and some classes of promoters, and depleted in repressed and repetitive states.

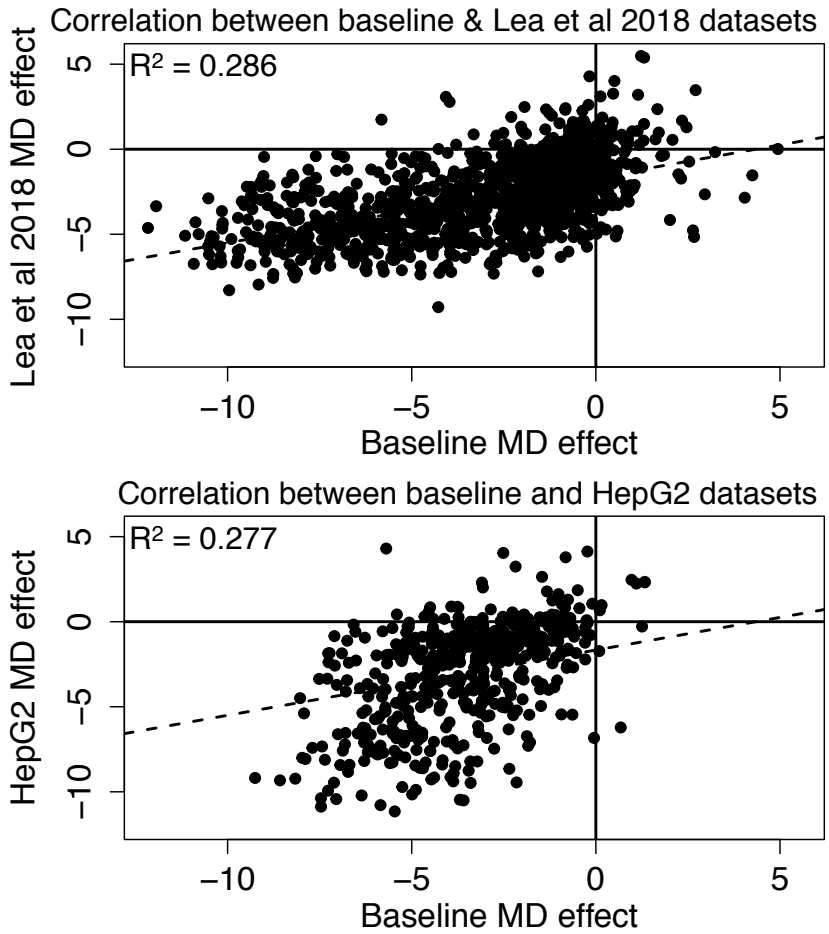

Figure 1-figure supplement 8. Methylation-dependent regulatory activity across datasets. Effects of methylation on regulatory activity estimated in this study in the baseline dataset are consistent with methylation effects in K562s estimated from a previously generated mSTARR-seq dataset (Lea *et al*., 2018) and with methylation effects estimated in HepG2 liver cells (Lea *et al*., 2018: Pearson's r = 0.534 for 1250 windows with FDR < 1% in both data sets, $R^2 = 0.286$, p = 3.19×10^{-93}; HepG2: Pearson's r = 0.526 for 511 windows with FDR < 1% in both data sets, $R^2 = 0.277$, p = 8.87×10^{-38}). Each dot represents a 600 bp regulatory window identified, in either the sham or methylated states, in both datasets (FDR < 1%; note that not all regulatory windows show significant methylation dependence [MD]). Dashed lines are the best fit lines. In all cases, negative effect sizes correspond to reduced activity in the methylated condition and positive effect sizes correspond to increased activity in the methylated condition.

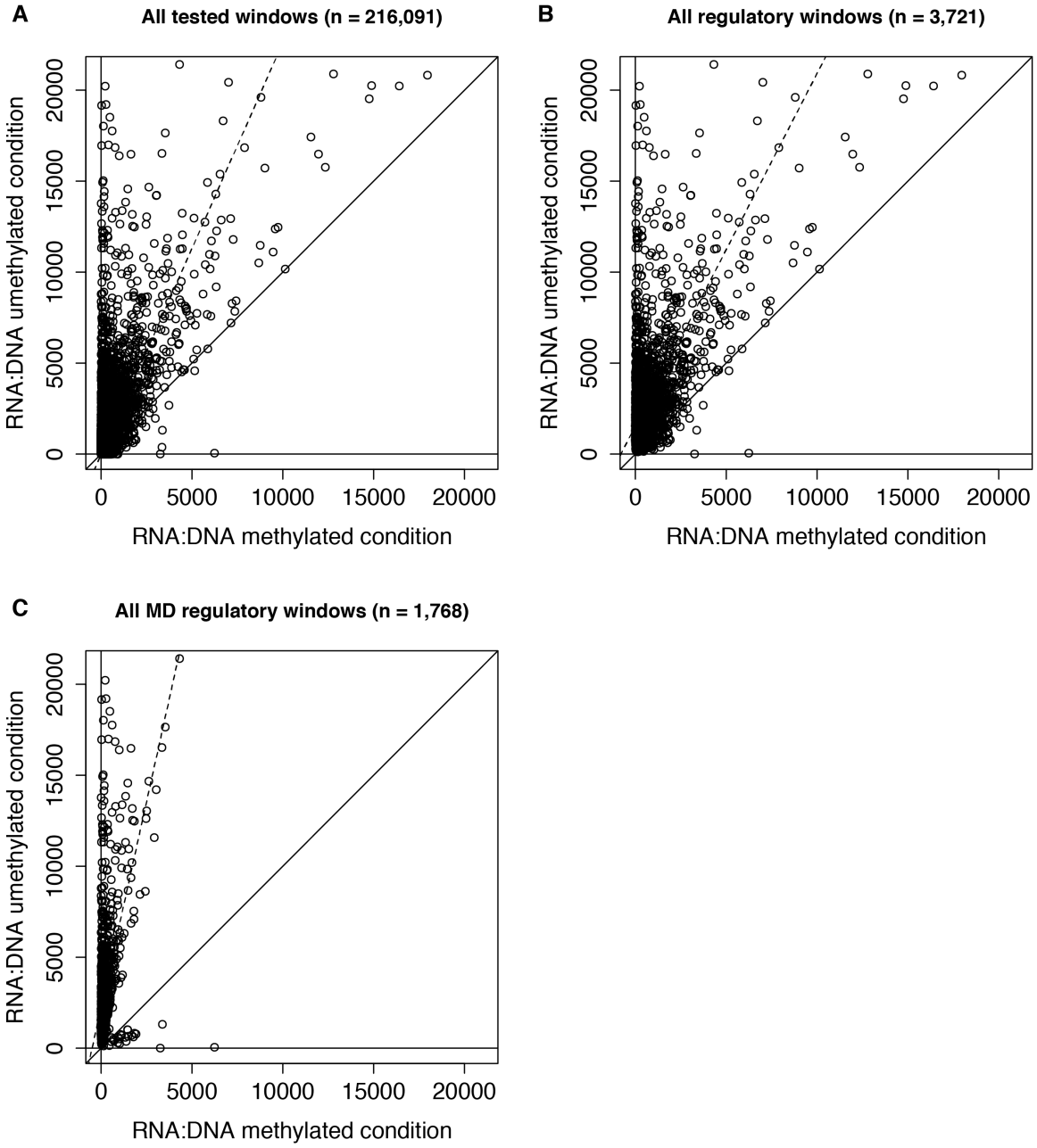

Figure 1-figure supplement 9. RNA to DNA ratios in the methylated and unmethylated replicates in the baseline dataset. Mean RNA (in counts per million) to DNA ratios formethylated replicates (x-axis) versus unmethylated replicates (y-axis). A constant of 0.5 was added to the initial raw counts to ensure no denominator values were 0. Each dot represents a 600 bp window that was formally tested for enhancer activity (**A**), exhibited significant regulatory activity (**B**), or exhibited significant methylation-dependent regulatory activity (**C**) in the baseline dataset. Solid diagonal lines represent y = x, and dashed lines represent the best fit lines. As expected, 600 bp windows tend to show higher RNA to DNA ratios in the unmethylated condition relative to the methylated condition.

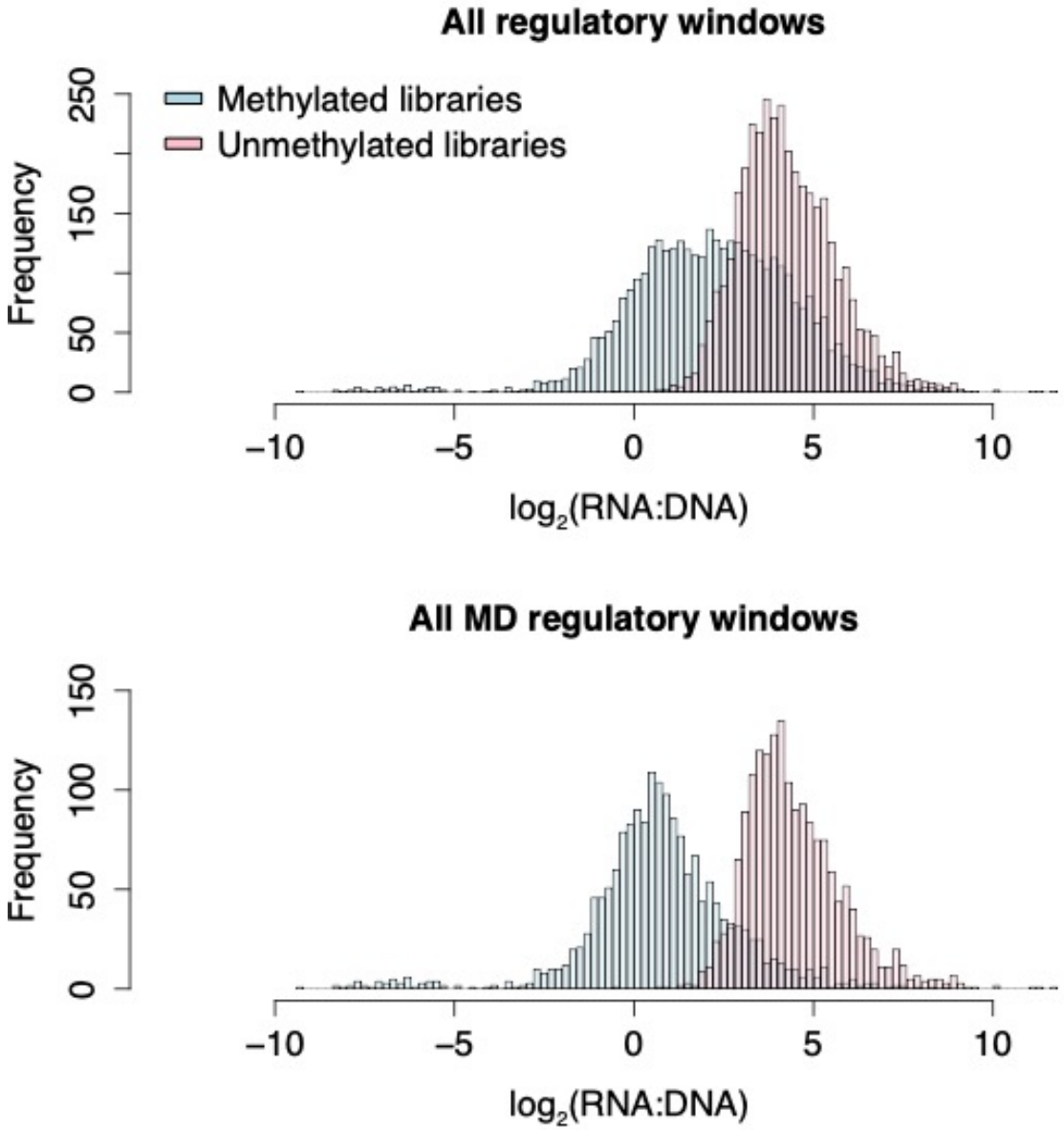

Figure 1-figure supplement 10. Histograms of RNA to DNA ratios in the baseline dataset. The x-axis represents the $\log_2$(mean RNA [in counts per million] to DNA ratios) for the baseline dataset. A constant of 0.5 was added to the initial raw counts to prevent 0 from being in the denominator. Lower values on the x-axis indicate windows showing lower regulatory activity.

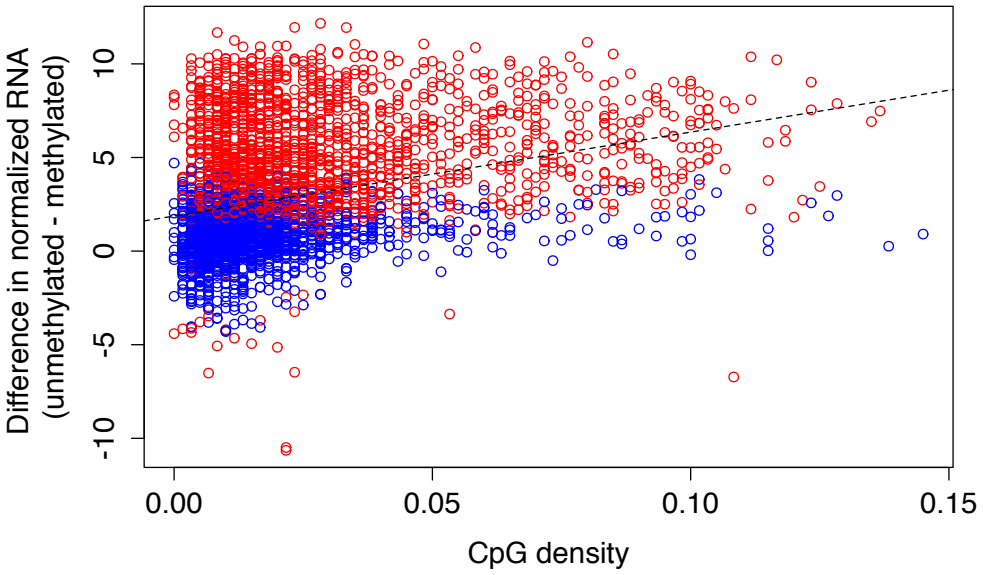

Figure 1-figure supplement 11. Relationship between CpG density and methylation-dependent regulatory activity. CpG-dense mSTARR-seq regulatory regions are more likely to be repressed by DNA methylation (positive y-axis value; Spearman's rho = 0.370, p = 9.865 x 10^{-121}; n = 3,721 regions with mSTARR-seq regulatory activity). Each dot represents a 600 bp window that showed significant regulatory activity (FDR < 1%). Red and blue dots represent regulatory windows where methylation-dependent activity was or was not detected, respectively. The dashed line represents the best fit line.

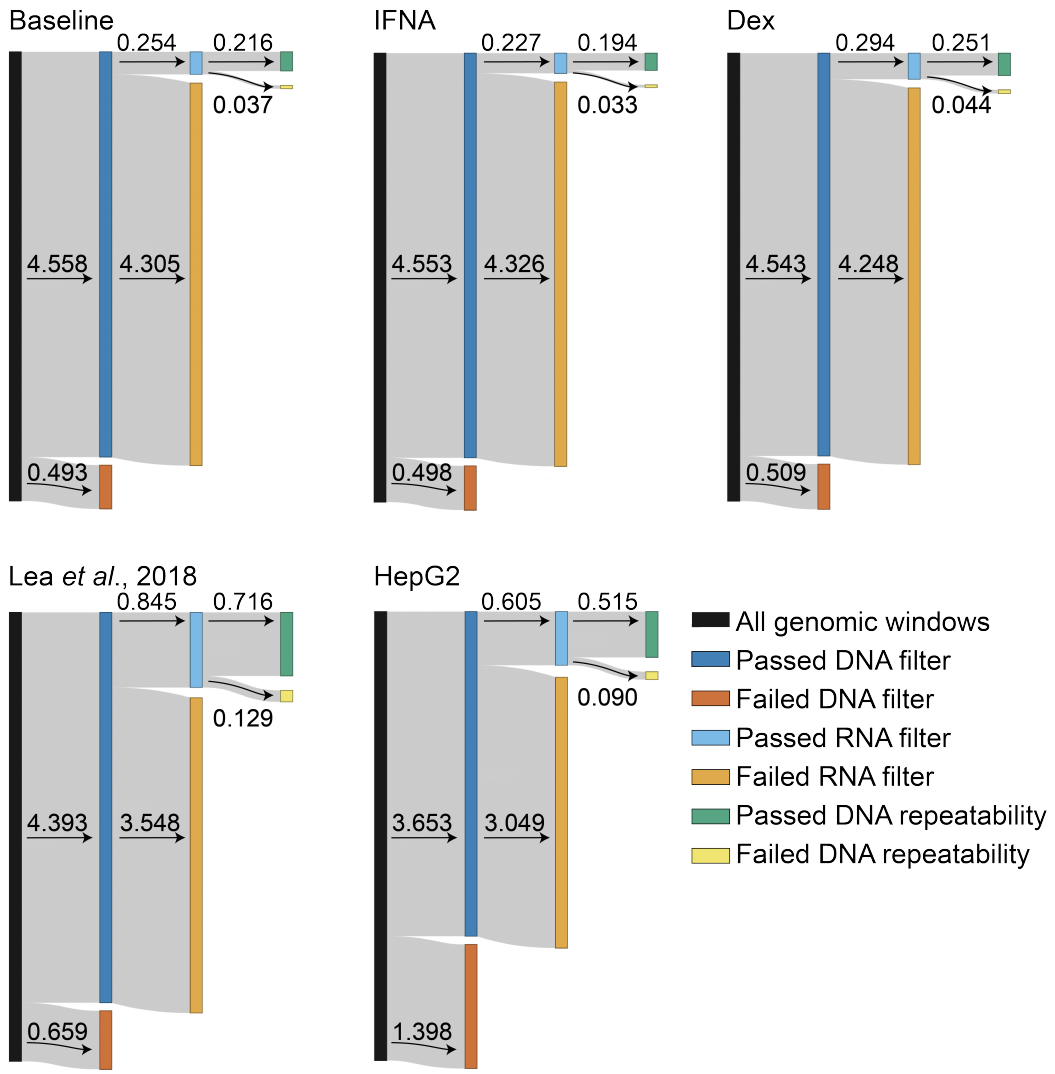

Figure 2-figure supplement 1. Filtering results across datasets. Each of the 5 datasets began with 5,051,776 600 bp genomic windows. For each of the 5 datasets, we reduced the dataset to windows that had nonzero counts in at least three DNA samples in the methylated condition *and* three DNA samples in the unmethylated condition (i.e., 6 DNA samples total; "DNA filter"). We then reduced the dataset to windows that had nonzero counts in at least three RNA samples in either the methylated *or* unmethylated condition ("RNA filter"). Finally, we retained only windows that showed high repeatability across DNA samples, following (Lea *et al*., 2018) ("DNA repeatability"). Numbers correspond to million windows that passed or failed each filter for which the arrow points to. Note that one mSTARR RNA-seq sample in the baseline condition [sample ID L31250] was removed from further analysis because it had an unusually high proportion of zero counts in the testable windows; we therefore also removed the corresponding paired DNA sample prior to analysis). See Supplementary File 9 for the precise window numbers corresponding to the plots.

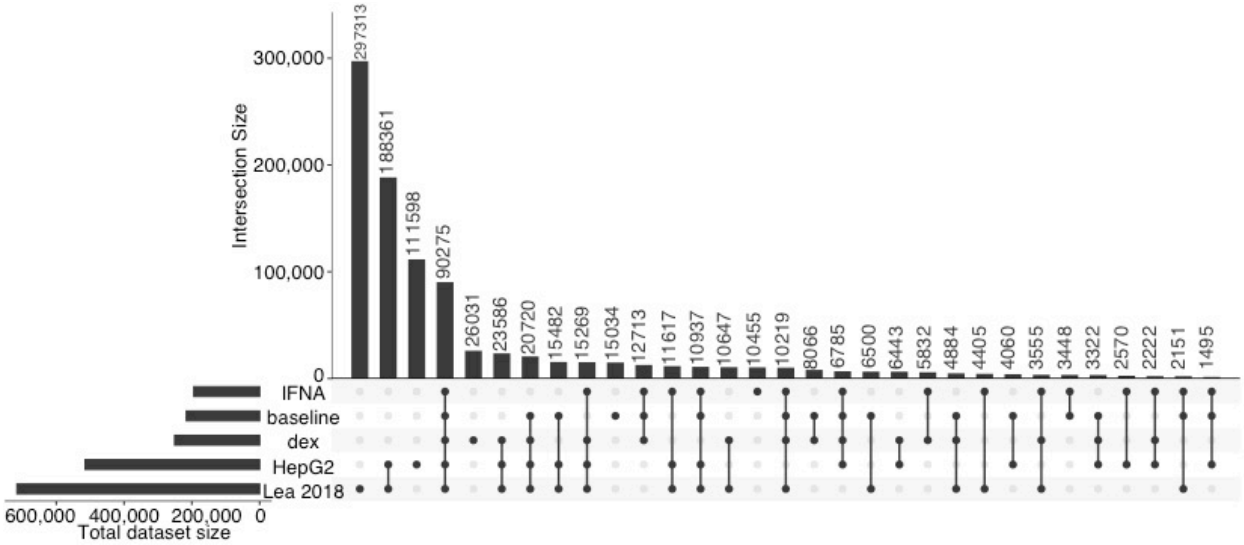

Figure 2-figure supplement 2. Overlap of tested genomic windows across datasets. Upset plots showing the degree to which 600 bp non-overlapping genomic windows are shared between five datasets (baseline null, IFNA, dex, HepG2, and Lea *et al*., 2018; all datasets were analyzed following the same pipeline). Note that the same input library was used in Lea *et al.*, 2018 and the HepG2 experiment, which differs from the library used here for baseline, dex, and IFNA experiments.

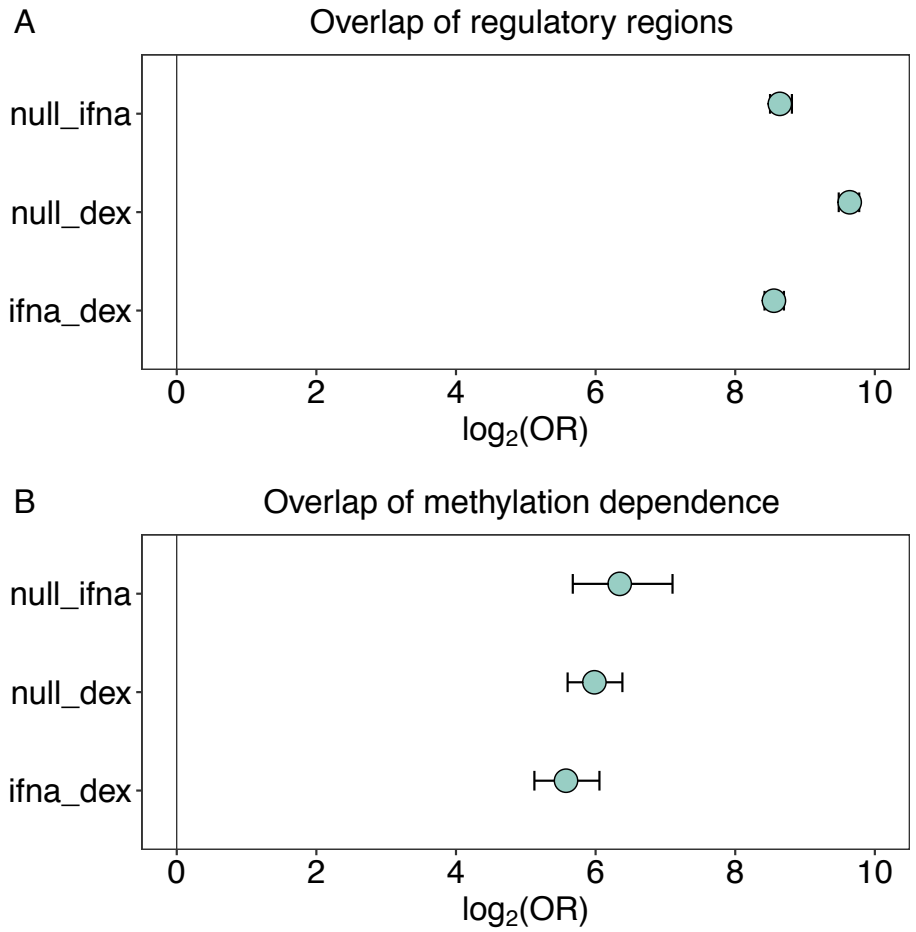

Figure 2-figure supplement 3. Overlap of regulatory activity and effects of methylation across environmental conditions. (A) Regulatory regions in the baseline condition are highly likely to retain regulatory activity upon challenge with IFNA or dex (IFNA $\log_2$(OR) [95% CI] = 8.639 [8.499, 8.812], $p < 1.0 \times 10^{-300}$; dex $\log_2$(OR) [95% CI] = 9.640 [9.483, 9.776], $p < 1.0 \times 10^{-300}$). Regulatory regions also significantly overlap between IFNA- and dex-challenged cells ($\log_2$(OR) [95% CI] = 8.554 [8.420, 8.698], $p < 1.0 \times 10^{-300}$). **(B)** Regulatory windows identified in two environmental conditions tend to share significant effects of DNA methylation on regulatory activity (i.e., interaction effects between methylation and regulatory activity) across the two environmental conditions (baseline and IFNA $\log_2$(OR) [95% CI] = 6.345 [5.673, 7.102], $p < 7.33 \times 10^{-239}$; baseline and dex $\log_2$(OR) [95% CI] = 5.982 [5.599, 6.384], $p < 1.0 \times 10^{-300}$; IFNA and dex $\log_2$(OR) [95% CI] = 5.576 [5.123, 6.055], $p < 4.70 \times 10^{-266}$).

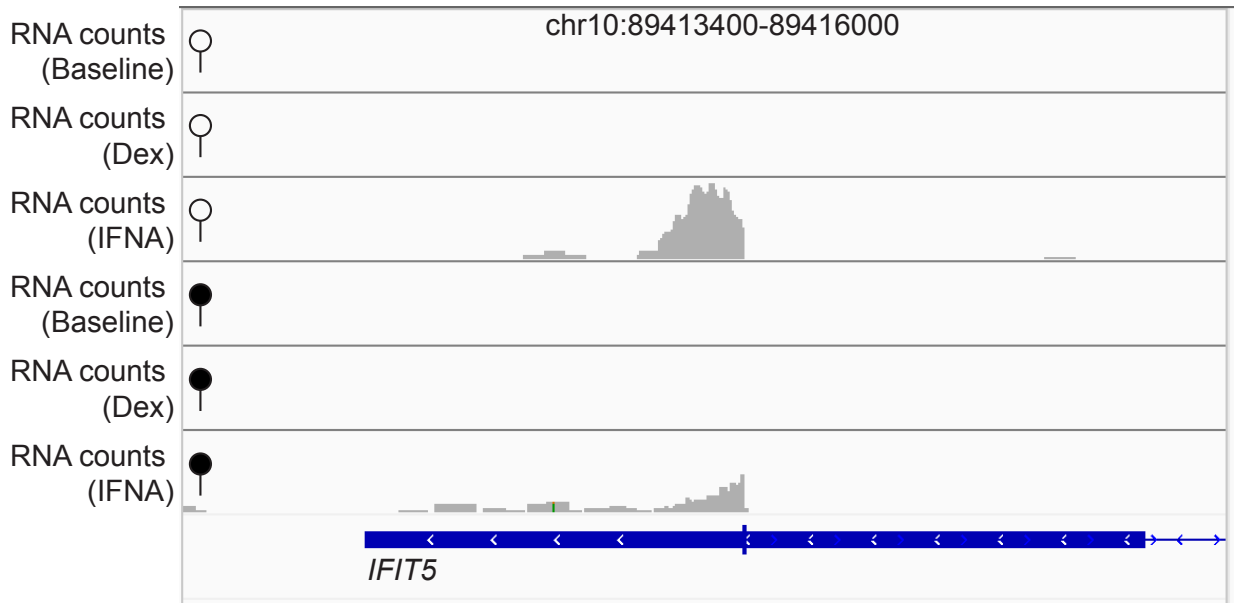

Figure 2-figure supplement 4. *IFIT5* endogenous gene expression is responsive to IFNA stimulation. Tracks show non-normalized, raw read pile-ups of endogenous *IFIT5* (ENSG00000152778) gene expression in either the unmethylated (open circle) or methylated (filled circle) condition, with all y-axis maximums set to 100. The replicates for endogenous gene expression shown here are the same replicates used for measuring regulatory activity shown in Figure 2A. *IFIT5* is only detectably expressed after IFNA stimulation (note that the difference in peak heights between the IFNA-stimulated unmethylated and methylated conditions is because the plot shows raw reads; there is no effect of methylation treatment on endogenous *IFIT5* gene expression after normalization for library size: $p = 0.489$).

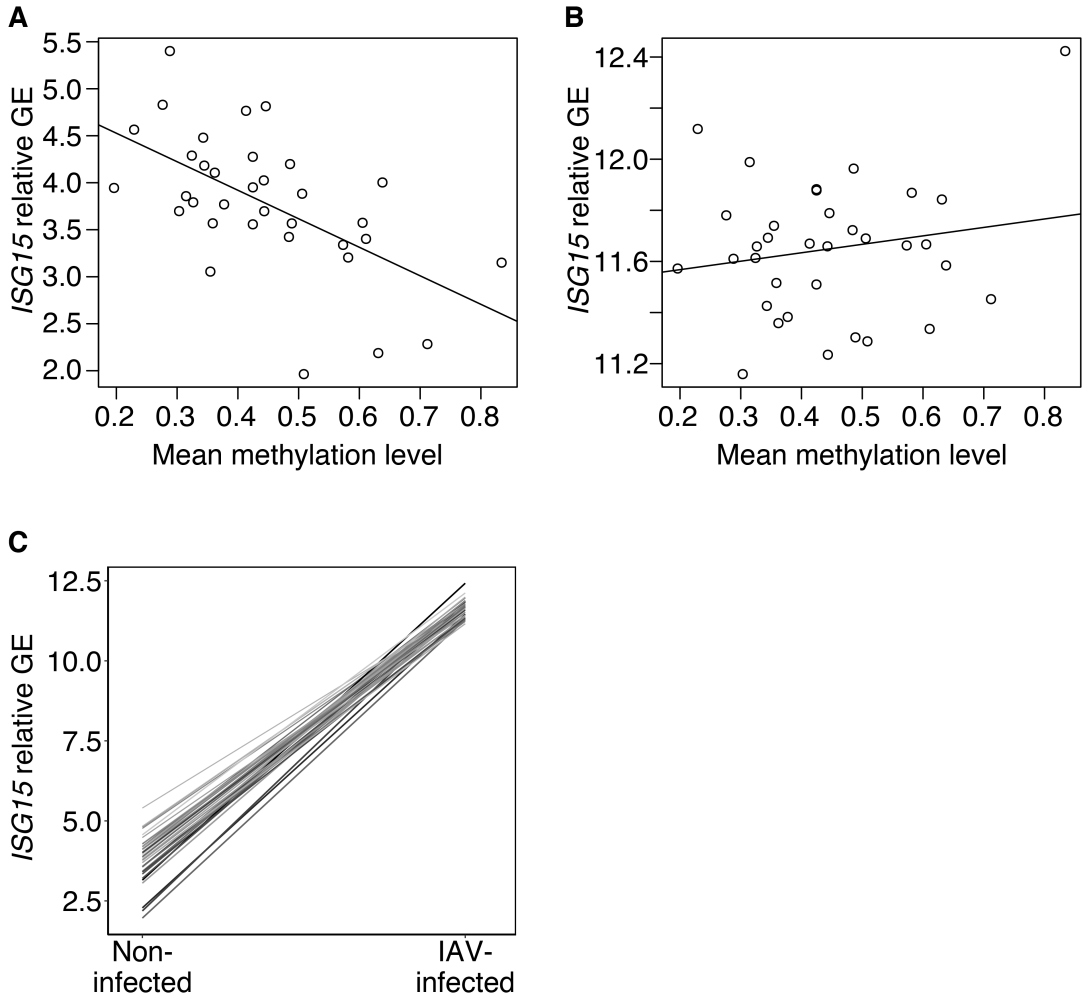

Figure 3-figure supplement 1. Across individuals, methylation in the mSTARR-seq annotated enhancer chr1:1013400-1014000 predicts the *ISG15* gene expression response to flu. (A) Across individuals, average methylation within the mSTARR-seq annotated enhancer chr1:1013400-1014000 in non-infected baseline macrophages significantly predicts *ISG15* gene expression (GE) in the non-infected condition ($R^2 = 0.324$, $p = 2.66 \times 10^{-4}$), but **(B)** not in the IAV-infected condition ($R^2 = 0.001$, $p = 0.316$). Each dot represents an individual. Relative GE is log(CPM) after regressing out the effects of sequencing batch, age, and admixture. **(C)** Individuals with relatively low methylation in the mSTARR-seq chr1:1013400-1014000 enhancer (indicated by lighter line color) in the baseline, non-infected condition tend to have higher *ISG15* gene expression in the non-infected condition, ultimately resulting in a shallower *ISG15* transcriptional response to IAV infection (as indicated by slope of the line). Each line represents an individual.

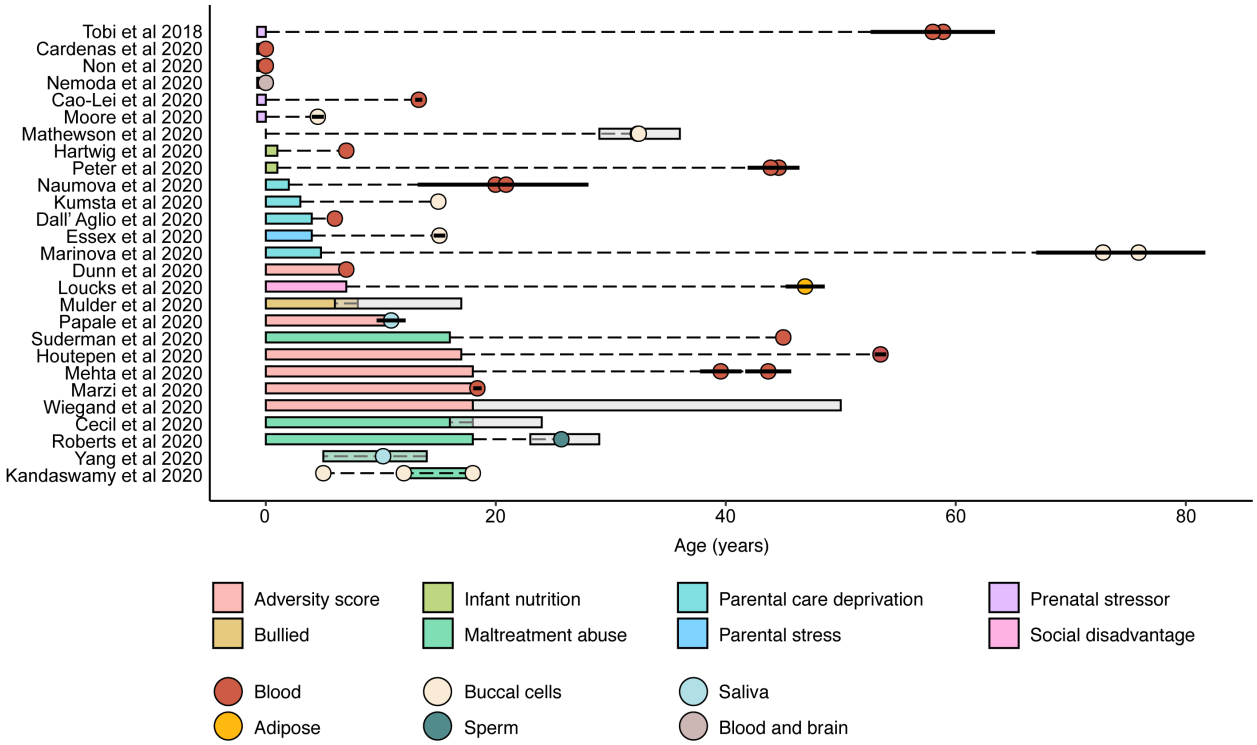

Figure 4-figure supplement 1. Summary of early-life adversity (ELA) studies. Colored rectangles indicate ranges of age at adversity. Circles represent mean ages at sample collection and are colored according to the tissue type used to measure methylation levels. Ranges and standard errors of ages at sample collection, when reported, are indicated by gray rectangles and horizontal black solid lines, respectively. See Supplementary File 20 for results of Fisher's exact tests assessing enrichment of ELA-associated CpGs for regulatory activity.